GABAergic plasticity in neuronal circuits of fear

Inauguraldissertation

zur Erlangung der Würde eines Doktors der Philosophie
vorgelegt der
Philosophisch-Naturwissenschaftlichen Fakultät der Universität Basel
von

Elisabeth Vogel

aus Wien, Österreich

Basel 2015

Genehmigt von der Philosophisch-Naturwissenschaftlichen Fakultät auf Antrag von

Prof. Dr. Andreas Lüthi

Fakultätsverantwortlicher und Dissertationsleiter

Prof. Dr. Josef Bischofberger

Koreferent

Basel, den 24.3.2015

Prof.Dr. Jörg Schibler

(Dekan)

TABLE OF CONTENTS

1. ABBREVIATIONS

2-AG	2-arachidonoylglycerol
ACSF	artificial cerebrospinal fluid
AMPA	α-amino-3-hydroxy-5-methyl-4-isoxazolepropionic acid receptor
ANOVA	analysis of variance
AP	action potential
BA	basal amygdala
BLA	basolateral amygdala
BMA	basomedial amygdala
BSA	bovine serum albumin
BZ	benzodiazepine
CB	calbindin
CB1R	cannabinoid receptor-1
CCK	cholecystokinin
CCK_L	large CCK expressing interneuron
CCK_S	small CCK expressing interneuron
CEA	central amygdala
CEl	central lateral amygdala
CElc	central capsular amygdala
CEm	central medial amygdala
CNQX	6-cyano-7-nitroquinoxaline-2,3-dione
CR	calretinin
CS	conditioned stimulus
DGLα	diacylglycerol lipase α

DSI	depolarization induced suppression of inhibition
eCB	endocannabinoid
E-face	ectoplasmic face
E/I ratio	ratio between excitation and inhibition
fAHP	fast after hyper polarization
Flp	flippase
FRIL	freeze-fracture replica immunolabeling
GABA	γ-aminobutyric acid
GAD65	65 kD iso-form of the GABA synthesizing enzyme glutamic acid decarboxylase
GAD67	67 kD iso-form of the GABA synthesizing enzyme glutamic acid decarboxylase
GFP	green fluorescent protein
IL	infralimbic region in medial prefrontal cortex
I-LTP	long-term potentiation at inhibitory synpses
IMP	intramembrane particle
IPSC	inhibitory postsynaptic current
ITC	intercalated cell cluster
LA	lateral amygdala
LTD	long-term depression
LTP	long-term potentiation
MGL	monoacylglycerol lipase
mIPSC	miniature inhibitory postsynaptic current
mPFC	medial prefrontal cortex
NGS	normal goat serum

NMDA	N-methyl-D-aspartate
P-face	protoplasmic face
PL	prelimbic region in medial prefrontal cortex
PLC	phospholipase C
PN	pyramidal neuron
PN_{IL}	infralimbic region projecting pyramidal neuron
PN_{PL}	prelimbic region projecting pyramidal neuron
PSA	postsynaptic area
PTX	picrotoxin
PV	parvalbumin
R_{input}	input resistance
SDS	sodium lauryl sulfate
SOM	somatostatin
STP	short-term plasticity
TBS	tris-buffered saline
TTX	tetrodotoxin
US	unconditioned stimulus
VGAT	vesicular GABA transporter
VIP	vasointestinalpeptide
vlPAG	ventro-lateral periaquaeductal grey
V_m	resting membrane potential
VTA	ventro tegmental area
WIN	WIN55,212-2

2. ABSTRACT

Neuronal circuits of fear and anxiety have been studied extensively not only to understand basic principles underlying anxiety disorders but also to investigate mechanisms of learning and memory. Fear conditioning is a powerful model system of associative learning, where the animal learns that an initially neutral stimulus predicts a fearful event. A key brain structure in this experimental paradigm is the amygdala, located in the temporal lobe. Synaptic plasticity of amygdala principle neurons gained a lot of attention and it has been shown how converging inputs trigger strengthening of synaptic transmission, which molecular changes are involved and which glutamatergic cell types and output pathways are important for high fear and low fear states. However, network mechanisms balancing the activity of these pyramidal neurons remain poorly understood. It is conceivable that amongst other contributors, local GABAergic interneurons might be involved and undergo plastic changes with fear conditioning and extinction.

In my thesis I focused on how GABAergic transmission onto pyramidal cells is organized in fear circuits. First, in a broad approach and in collaboration with Yu Kasugai and Franceso Ferraguti from the Medical University Innsbruck, we show that fear conditioning induces functional and ultrastructural changes at inhibitory synapses. Following fear learning, GABAergic transmission is enhanced, which is correlated with an enlargement of synapses and a change in receptor subunit composition.

Second, in target specific experiments, I studied the dynamic regulation of inhibition from CCK expressing interneurons onto two functionally distinct classes of projections neurons. Data indicate that characteristics at these synapses facilitate asymmetric activity of particular pyramidal cell populations via retrograde endocannabinoid signaling and that inhibitory control is organized in a cell type specific manner.

3. INTRODUCTION

3. 1. Learning & memory

Throughout life we acquire knowledge about our environment. New information is encoded, can be stored and retrieved in neuronal circuits and allows us to adjust our behavior. Underlying mechanisms of learning and memory are based on experience dependent plasticity (Kandel et al., 2000). They involve structural and functional adaptations ranging from synapse formation and elimination to growth and retraction of dendritic spines and axonal boutons, to strengthening or weakening of existing synapses (Holtmaat & Svoboda, 2009; Caroni et al., 2012). Strengthening and weakening of existing synapses is mostly regulated by synaptic activity and leads to reversible or permanent molecular changes (Holtmaat & Svoboda, 2009). Reversible changes are believed to correlate with short-term memory, whereas permanent changes are referred to as long-term memory and are often accompanied by structural changes (Holtmaat & Svoboda, 2009).

3. 1. 1. Long-term potentiation

LTP (long-term potentiation), a cellular model of learning and memory, was used to study mechanisms of synaptic plasticity in acute brain slices for many decades (Nicoll & Malenka, 1995; Malenka & Bear, 2004; Sah et al., 2008; Granger & Nicoll, 2014). Various forms have been described at different synapses, however they are all defined by a long lasting increase in synaptic transmission following high frequency input stimulation. In associative NMDA (N-methyl-D-aspartate) receptor-dependent LTP two different input pathways are required to be active simultaneously (Kandel et al., 2000). Calcium influx through NMDA receptors is blocked by magnesium at the resting membrane potential. Therefore, the postsynaptic neuron needs to be activated to resolve the magnesium block. At the same time the second input activates NMDA receptors, calcium enters the neuron and triggers a cascade of events that lead to the insertion of new receptors at the synapse (Kandel et al., 2000). Thus, the NMDA receptor is a coincidence detector, as two separate sources are required to trigger the potentiation simultaneously. In an experimental setting, clamping the neuron in a depolarized state can substitute for the

depolarizing source of inputs. In addition to NMDA receptors, L-type voltage gated calcium channels can contribute to calcium influx (Bauer et al., 2002). Besides the number of postsynaptic receptors, spine size as well as the number of spines can be increased and together result in strengthening of synaptic transmission (Fig 1 A and B) (Lamprecht & LeDoux, 2004).

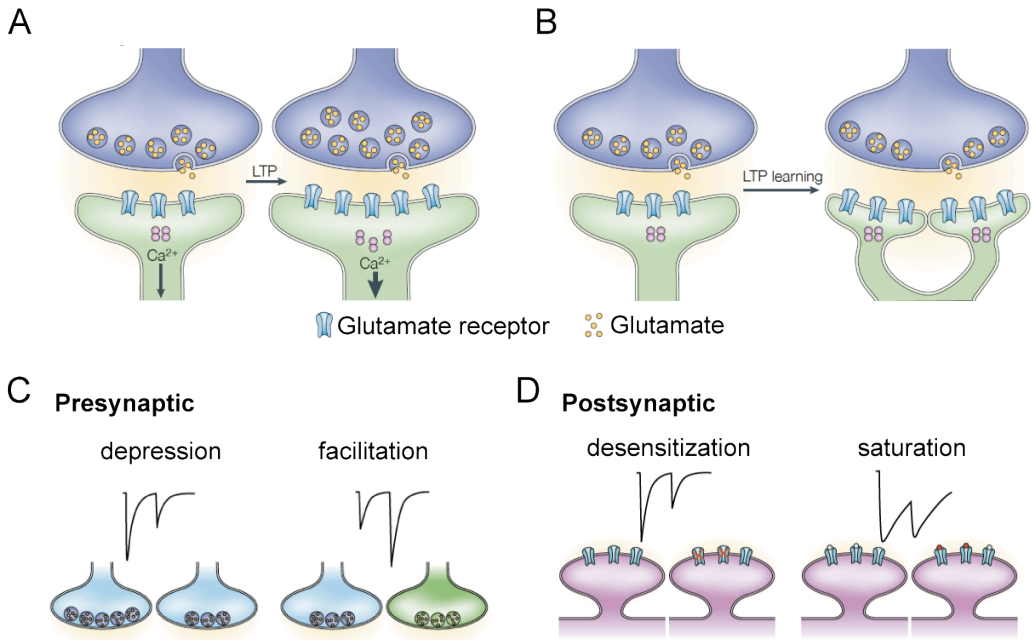

Figure 1: Schematic illustration of cellular correlations of LTP and STP (**A**) LTP can lead to an increase in spine size, number of neurotransmitter receptors, presynaptic vesicles, postsynaptic ribosomes and changes in calcium compartmentalization; (**B**) Alternatively LTP can enhance the number of spines, number of independent synaptic release sites and therefore increase synaptic transmission (adapted from Lamprecht & LeDoux, 2004). (**C**) Presynaptic mechanisms of short-term plasticity; schematized voltage clamp traces (top) illustrate depression and facilitation. At depressing synapses the first stimulation (left) can deplete the pool of readily releasable vesicles and therefore lead to smaller currents with the second action potential (right). At facilitating synapses a residual elevation in intracellular calcium (green shading), combined with the influx of calcium in response to the second stimulus, results in enhanced release. (**D**) Postsynaptic mechanisms leading to desensitization and saturation of postsynaptic currents. Desensitization can be due to receptors with high affinity for the transmitter. After the first stimulation a population of receptors can remain bound with transmitter (red circles) and therefore be unavailable to respond to the second stimulus. Saturation is often caused by channels with slow kinetics such as NMDA receptors. They can produce a large amount of current in response to a second stimulus. Although the second EPSC has smaller amplitude in absolute values, it is summated with the previous EPSC (adapted from Blitz et al., 2004).

Other forms of LTP drive the insertion of AMPA (α-amino-3-hydroxy-5-methyl-4-isoxazolepropionic acid receptor) receptors into the synapse and it has been shown that the incorporation of AMPA receptors is required for fear learning (Rumpel et al, 2005).

In contrast to LTP, LTD (long-term depression) weakens synaptic efficacy as a result of low frequency stimulation (Collingridge et al., 2010). Recently, a causal link between LTP, LTD and memory formation has been established by using optogenetic stimulation in an associative learning task. After auditory fear conditioning associative memory is impaired by LTD stimulation of auditory inputs, whereas LTP stimulation reactivates the memory (Nabavi et al., 2014).

Potentiation of inhibitory synapses is an important mechanism of circuit refinement but has received much less attention. Yet, a number of different forms involving various interneuron subtypes and pre- and postsynaptic expression mechanisms have been described (Castillo et al., 2011). I-LTP and I-LTD can have consequences on the probability of GABA release as well as on the number, sensitivity and responsiveness of $GABA_A$ receptors. Most forms of I-LTD also require a second source of stimuli, which is not GABAergic and may stem from excitatory synapses or retrograde messengers (Chevaleyre et al., 2006; Regehr et al., 2009; Castillo et al., 2011). This associative mechanism requires simultaneous presynaptic interneuron activity and postsynaptic excitation, which are then transformed into long-term plasticity. Interestingly, excitatory and inhibitory LTP can occur simultaneously via feed forward inhibition (Lamsa et al., 2005), which may be important for balancing the E/I ratio.

LTP is often associated with changes on a structural level. In general, it is conceivable that axonal plasticity can occur, however, most data stems from experiments involving brain injury (Spejo & Oliveira, 2014) or artificial long-term stimulation (Grubb & Burrone, 2010; Kuba et al., 2010) and so far a causal link between learning and axonal plasticity has not been established. First experiments on morphological changes at dendritic spines have been

conducted in aplysia during the 1980s (Bailey & Chen, 1983, 1988) reporting alterations in synaptic size and shape in response to long-term habituation and sensitization. Furthermore, a number of studies in hippocampus showed that LTP induces changes in spine number, the size of the spine head as well as widening and shortening of the spine neck (Lamprecht & LeDoux 2004). These modifications initiated 2 min after LTP stimulation and lasted up to 23h. More recent experiments give insight how *in vivo* learning processes correlate with rearrangements on a structural level. Data from independent groups (Xu et al., 2009; Yang et al., 2009) suggest that motor learning induces spine growth in motor cortex and that newly formed spines are stabilized with subsequent training. Moreover, fear conditioning, a form of associative learning increases the rate of spine elimination in mouse frontal association cortex whereas extinction of fear increases the rate of spine formation (Lai et al., 2012). Thus, it is imaginable that the formation and elimination of spines might be directly linked with the formation of new memory. Increases in number of spines as well as spine size might also be associated with a strengthening of synaptic transmission (Fig. 1A and B).

3. 1. 2. Short-term plasticity

While LTP and LTD form a persistent memory trace, short-term plasticity (STP) modulates synaptic transmission in the time range of seconds. Repeated stimulation of synaptic connections often results in gradual changes in postsynaptic response amplitudes (Fig 1C and D) (Blitz et al., 2004). These may either be facilitating or depressing and can be caused by pre- or postsynaptic factors. The underlying mechanisms may be dependent on calcium influx to presynaptic terminals, number of vesicles, receptor composition or physiological activity patterns. At some synapses short-term depression can be caused by a reduction of release probability and depletion of the readily releasable pool of vesicles. In other cases stimulation with the same frequency can increase local calcium levels and thereby enhance the probability of transmitter release leading to facilitated postsynaptic potentials (Blitz et al., 2004). Postsynaptic factors can also contribute to STP. Depending on receptor properties exposure to neurotransmitters can cause

receptor desensitization or saturation. In any case diverse STP dynamics lead to differentially timed input for the postsynaptic cell.

3. 1. 2. 1. Retrograde signaling in STP

Some forms of STP involve retrograde messengers, such as endocannabinoids (eCBs), which are released by the postsynaptic cell (Ohno-Shosaku et al., 2001; Wilson & Nicoll, 2001; Wilson et al., 2001). Endocannabinoids are a group of lipophilic molecules that are highly abundant and believed to be major contributors of synaptic plasticity (Luchucchi & Pistis, 2012). An activation of the postsynaptic cell via mGluRs, depolarization or stimulation of excitatory afferents triggers the production of diacylglyercol (DAG) by phospholipase C (PLC). Diacylglycerol lipase α (DGLα) converts DAG to the major eCB, 2-AG, which is released from the postsynaptic cell and travels back across the synapse to bind at G-protein-coupled type 1 cannabinoid receptors (CB1Rs) on presynaptic terminals. As a consequence, calcium influx is inhibited, potassium channels are activated leading to a hyperpolarization of the terminal and thus the probability of transmitter release decreased (Chevaleyre et al., 2006).

Depolarization-induced suppression of inhibition (DSI) is a common mechanism of distinct GABAergic synapses from CB1R-expressing CCK basket cells onto pyramidal neurons (Ohno-Shusako et al., 2001; Wilson et al., 2001; Wilson & Nicoll, 2001; Yoshida et al., 2011). A postsynaptic activation and eCB release reversibly blocks coincident inhibitory input from CCK interneurons in the time range of seconds. Also at excitatory synapses this retrograde signaling mechanism can be found to suppress glutamatergic input (DSE, depolarization induced suppression of excitation) (Wilson & Nicoll, 2002; Diana & Marty, 2004; Yoshida et al., 2011). The eCB synthesis enzyme DGLα is expressed in high levels in the somatic region of pyramidal cells and in lower levels in dendrites (Chevaleyre et al., 2006). Endocannabinoids are believed to play important roles in memory and cognition and specifically in fear extinction learning.

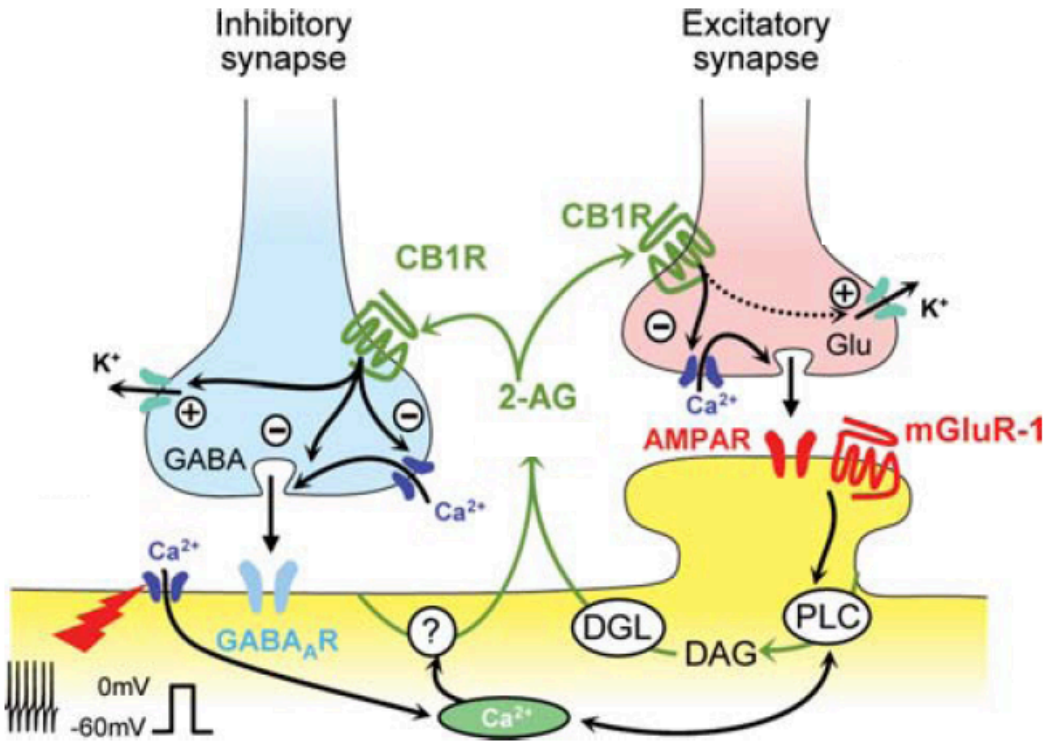

Figure 2: Schematic illustration of retrograde endocannabinoid signaling at inhibitory and excitatory synapses. The release of 2-AG can be triggered by postsynaptic activation via excitatory afferents, activation of mGluRs or depolarization by the experimenter. DGLα is converted to the main endocannabinoid 2-AG by DAG and PLC. 2-AG binds to presynaptic G-protein coupled CB1Rs, inhibits calcium influx and activates potassium channels. As a consequence the probability of transmitter release is decreased (adapted from Chevaleyre et al., 2006).

3. 1. 3. Excitation/inhibition balance

An additional factor contributing to plasticity of neuronal networks is the ratio between excitation and inhibition. During sensitive periods, developmental time windows when the effect of experience on the brain is particularly strong, even small shifts in the relative amount of excitation and inhibition can lead to alterations in plasticity (Hensch, 2005). Enhancing inhibition by administration of benzodiazepines directly after eye opening results in a premature onset of the critical period for ocular dominance (Fagiolini & Hensch, 2000). In mice lacking GAD65 ocular dominance plasticity is prevented but can be rescued by administration of diazepam (Hensch et al., 1998). However, not all GABAergic interneurons or $GABA_A$ receptors have impact on the regulation of critical periods (Hensch, 2005) and the dissection of these diverse neuronal

populations is important for understanding circuit mechanisms underlying learning processes.

In the amygdala it has been shown that the stimulation of glutamatergic projections from prelimbic (PL) and infralimbic (IL) subdivisions of the mPFC recruit excitation and feed-forward inhibition in basal amygdala principle neurons. Interestingly, after conditioning the E/I-balance is shifted towards excitation specifically in the $mPFC_{PL}$→amygdala pathway but not in $mPFC_{IL}$→amygdala micro-circuits (Arruda-Carvalho & Clem, 2014). This mechanism may encode fear memory by a pathway-specific enhancement of mPFC→amygdala transmission.

3. 2. Fear conditioning

A powerful model system that has been extensively studied to understand network mechanisms of learning and memory is auditory fear conditioning (LeDoux, 2000; Maren & Quirk, 2004; Fanselow & Poulos, 2005; Herry & Johansen, 2014). In this form of associative learning a neutral stimulus, a tone is paired with an aversive stimulus, an electric foot shock (unconditioned stimulus, US). After a few tone/shock pairings, presentation of the previously neutral stimulus alone (conditioned stimulus, CS) elicits aversive behavior (Fig. 3).

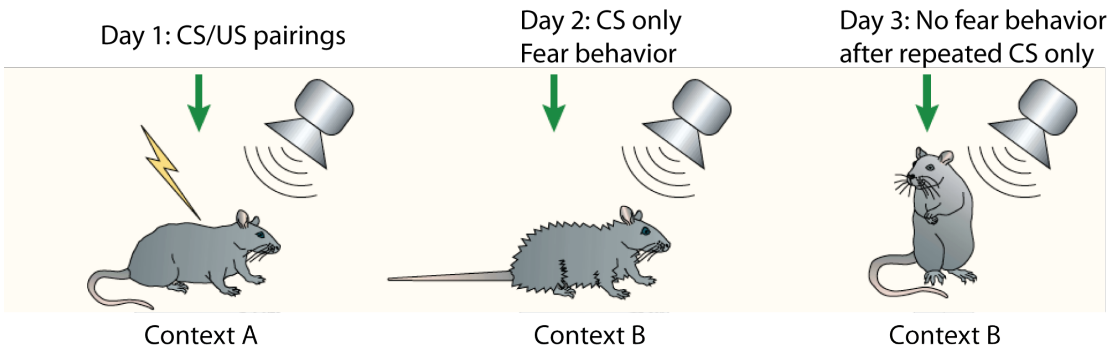

Figure 3: Auditory fear conditioning; during conditioning day 1 the animal receives pairings of a neutral tone (conditioned stimulus, CS) and a mild foot-shock (unconditioned stimulus, US) in the conditioning context. On the next day the animal is placed in another box with different light conditions, floor, smell and background noise. When the tone is now presented alone without a foot-shock the animal will react with freezing, a form of aversive behavior. After repeated presentations of the tone without reinforcing the US, conditioned fear will be extinguished and the animal learns that the tone is safe again (adapted from Nadel & Land, 2000).

Depending on intensity and proximity of the stimulus and also the nature of the context, aversive behaviors can be active or passive. In a closed experimental context the mouse usually responds to fearful stimuli with freezing. This innate defensive behavior evolved to avoid discovery by predators (LeDoux, 2000; Fanselow & Poulos, 2005) and can be measured by the absence of movement. Repeated presentations of the tone without a foot shock leads to extinction of conditioned fear and the animal learns that the tone is safe. Extinction is not an erasure of fear memory but an active learning process (Myers & Davis, 2007; Quirk & Mueller, 2008; Herry et al., 2010).

3. 3. The amygdala

The amygdala, a non-layered structure located in the medial temporal lobe, has been identified as a key brain area for fear and extinction learning (LeDoux, 2000; Maren & Quirk, 2004; Fanselow & Poulos, 2005; Herry & Johansen, 2014). It consists of several subnuclei with different cytoarchitecture. Lateral (LA), basal (BA) and basomedial amygdala (BMA) are often summarized and referred to as basolateral complex of the amygdala (BLA). It is a cortex-like structure with the majority of cell types being glutamatergic, intermingled with a minority of local GABAergic interneurons (15-20 %) (Aggleton, 2000). In contrast, the central amygdala (CEA) is striatum-like, mainly composed of inhibitory neurons. It comprises three subnuclei, central lateral (CEl), central capsular (CElc) and central medial amygdala (CEm). Additionally, three clusters of intercalated cells exist which are GABAergic (Fig. 4) (Aggleton 2000).

Amygdala subnuclei are highly interconnected. Furthermore, strong connections can be found with many other cortical and subcortical brain regions (Aggleton, 2000). During fear conditioning sensory information about CS and US from thalamus and cortex converge in the lateral amygdala, get processed in the basolateral nucleus and conveyed to central amygdala, the main output structure. It sends GABAergic long-range projections to the vlPAG, which are believed to mediate fear behavior (Herry & Johansen, 2014). The BA projects strongly to prelimbic (PL) and infralimbic (IL) regions

of the medial prefrontal cortex (mPFC) which are believed to play important roles in the expression of fear and extinction memory (Quirk & Mueller, 2008; Burgos-Robles et al., 2009; Sierra-Mercado et al., 2011). Furthermore, ITCs are believed to relay feed-forward inhibition to BLA and CEA (Ehrlich et al., 2009).

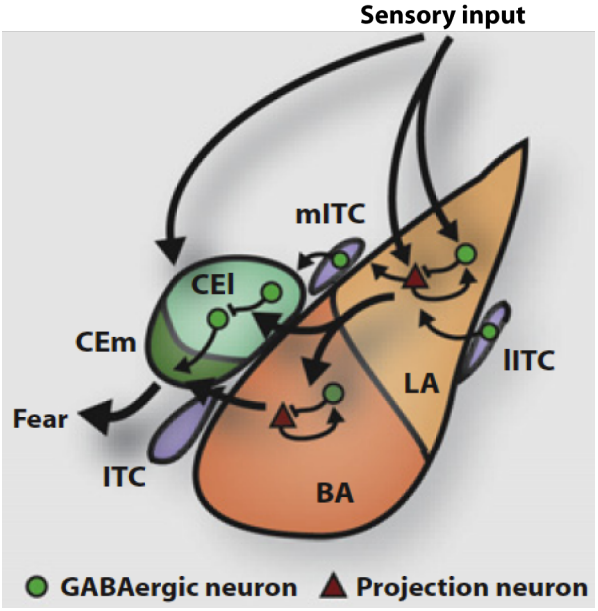

Figure 4: Simplified illustration of amygdala subnuclei and their interconnectivity. Lateral amygdala receives sensory input from thalamus and cortex, which is conveyed and processed in the basal amygdala. The central amygdala is the main output structure and sends long-range projections to vlPAG. Intercalated subnuclei are believed to relay feed-forward inhibition to BLA and CEA (adapted from Ehrlich et al., 2009).

3. 3. 1. Amygdala principle neurons

Amygdala principal neurons (PNs) can be differentiated by activity patterns and projection targets (Herry et al., 2008; Senn et al, 2014). Two functionally distinct classes were identified, fear and extinction neurons (Herry et al, 2008). While fear neurons were not responsive to tone presentations in unconditioned animals, they showed increased firing rates when the tone was presented during and after fear conditioning. Repeated tone presentations in turn, caused a loss of CS evoked firing. Contrary to fear neurons, extinction neurons became tone responsive only during extinction learning, when the CS was presented repeatedly without being paired with a foot shock. Interestingly,

fear neurons project to the prelimbic (PL) region of the mPFC, whereas extinction neurons project to the infralimbic (IL) subdivision. These mPFC subnuclei are believed to have opposing roles in fear behavior. Whereas PL is important for fear expression, the IL subdivision has been implicated in extinction memory consolidation and retrieval (Quirk & Mueller, 2008; Burgos-Robles et al., 2009; Sierra-Mercado et al., 2011). Consistently, basal amygdala PL-projecting PNs (PN_{PL}s) are activated when the animal is in a state of high fear, whereas IL-projecting PNs (PN_{IL}s) increase their activity in low fear states, such as with acquisition of extinction (Senn et al., 2014). The balance of activity between these two output pathways plays an important role in extinction learning. However, underlying circuit mechanisms remain unknown. Besides other factors it is conceivable that local inhibitory interneurons contribute to the modulation of activity between defined populations of projection neurons.

3. 3. 2. Interneurons in the amygdala

Many basal amygdala interneurons can be identified by morphology, activity pattern and marker expression, with analogies to previously described interneurons in hippocampus and cortex (Klausberger & Somogyi, 2008; Capogna, 2014). However, the diversity of basal amygdala GABAergic neurons has not been fully explored yet. The most numerous population consists of parvalbumin (PV) expressing interneurons (Fig. 5), which preferentially target the somatic region (PV-basket cells) or axon initial segment (axo-axonic cells) of postsynaptic neurons and can usually be characterized by a fast-spiking, non-adapting firing pattern (Rainnie et al., 2006; Muller et al., 2006). Cholecystokinin (CCK) interneurons can be divided in two main subgroups. Cells with small soma size (CCK_Ss) co-express calretinin (CR) and/or vasointestinalpeptide (VIP) (Mascagni & McDonald 2003) and target somatic and dendritic regions, whereas large CCK interneurons (CCK_Ls) stain positive for presynaptic CB1Rs and represent classical basket cells (McDonald & Mascagni, 2001; Katona et al., 2001). Another interneuron population expresses somatostatin (SOM) and selectively targets dendrites (McDonald & Mascagni, 2002; Muller et al., 2007).

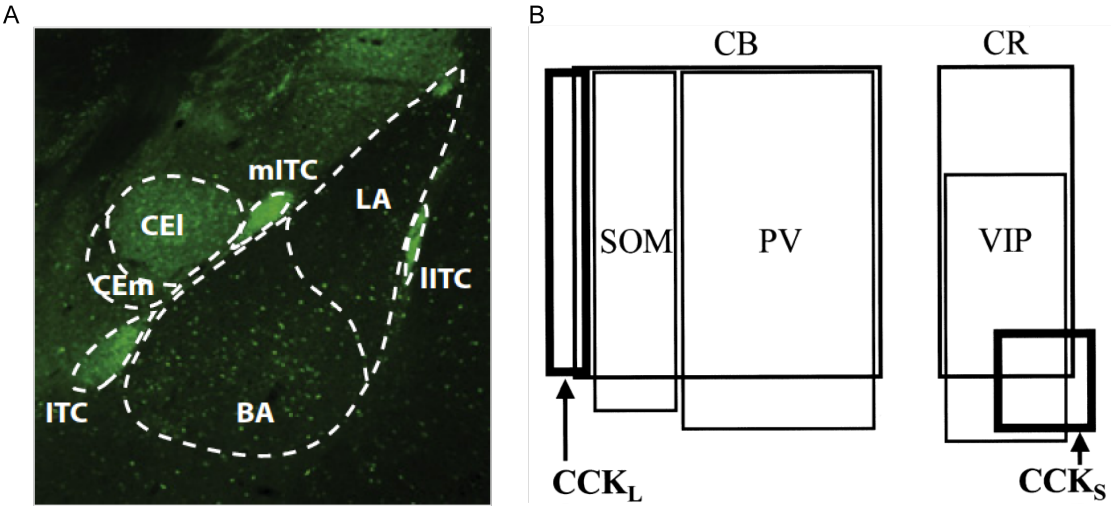

Figure 5: Interneurons in amygdala (**A**) Staining for the GABA synthesizing enzyme GAD67; The BLA is a cortex-like structure with a minority of GABAergic interneurons. The central amygdala is a striatum-like brain nucleus. Intercalated GABAergic cell clusters can be found at the border of the BLA (adapted from Ehrlich et al., 2009). (**B**) Interneuron subtypes in basal amygdala; CB calbindin, PV parvalbumin, SOM somatostatin, CR calretinin, VIP vasointestinal peptide, CCK_L large cholecystokinin expressing interneurons, CCK_S small cholecystokinin expressing interneurons (adapted from Mascagni & McDonald, 2003).

3. 4. The role of GABAergic inhibition in fear learning

The postsynaptic $GABA_A$ receptor is a pentameric ion channel consisting of five subunits arranged around a central chloride pore. Seven subunit classes with at least 18 different subtypes have been identified, however, most $GABA_A$ receptors in the CNS are heteropentamers composed of two α, two β and one γ subunit (Sieghart & Sperk, 2002). Depending on subunit composition $GABA_A$ receptors are susceptible to modulation by different benzodiazepines, which bind at the interface between α and γ_2-subunits. Benzodiazepines have been used extensively to treat anxiety disorders and are able to inhibit fear memory acquisition, consolidation and extinction (Makkar et al., 2010). Furthermore, it is indicated that certain subunits, such as α_2 mediate anxiolyis, whereas drugs selective for $GABA_A$ receptors containing the α_1 subunit have sedating effects but do not influence anxiety (Möhler, 2007). Therefore, not only interneuron subtypes but also the postsynaptic expression of distinct $GABA_A$ receptors might play a role in fear and extinction learning.

A number of *ex vivo* studies provide circumstantial evidence for changes in GABAergic inhibition following fear conditioning and extinction (Chhatwal et al., 2005; Heldt & Ressler, 2007). In these studies, it was shown that fear conditioning leads to a decrease in the overall surface levels of $GABA_A$ receptors and in a decrease in the mRNA and protein levels of gephyrin, a protein that is involved in the clustering of $GABA_A$ receptors at synapses. Conversely, fear extinction increased surface $GABA_A$ receptor expression and gephyrin levels. These findings suggested that bidirectional modulation of GABAergic inhibition may contribute to fear conditioning and extinction. The physiological consequences for GABAergic synaptic mechanisms are, however, not known. In the first part of my thesis I addressed this question by recording mIPSCs in amygdala PNs after fear conditioning and extinction to explore whether behavioral training induces changes in GABAergic transmission.

Furthermore, CCK interneurons have been implicated to play a role in fear and extinction behavior (Freund, 2003). Specifically, it was suggested that a CB1R mediated decrease of activity in local inhibitory networks within the BLA might dis-inhibit principal neurons and contribute to extinction of conditioned fear (Marscano et al., 2002). Large CCK interneurons (CCK_Ls) are the only interneuron subtype in amygdala expressing presynaptic CB1Rs. CB1R deficient mice exhibit impaired extinction behavior, however freezing levels after conditioning are not different from wild type animals (Marsicano et al., 2002). Interestingly, CB1Rs are highly co-localized with the expression of CCK, a neuropeptide, which is anxiogenic in humans. Intracerebroventricular injections of the CCK2 receptor agonist pentagastrin in mice inhibited the extinction of conditioned fear (Chhatwal et al., 2009). It is not understood how CCK and the endocannabinoid system are interacting but data indicates that CCK may activate a complex network of excitatory and inhibitory neurons within the BLA via interaction with CB1Rs (Bowers & Ressler, 2015).

Novel techniques such as optogenetic manipulation of genetically targeted subpopulations of interneurons in combination with unit recordings allowed further dissection of GABAergic circuits in learning and memory. Wolff and

colleagues (2014) have shown that PV and SOM interneurons bidirectionally control the acquisition of fear via a disinhibitory mechanism. During CS presentations PV interneurons are activated and thereby inhibit dendrite targeting SOM interneurons. As a consequence pyramidal cell dendrites are disinhibited which promotes CS/US associations. This is an elegant example of how subpopulations of interneurons have distinct functions in microcircuits and are capable of regulating neuronal activity in learning paradigms. It is likely that the large variety of GABAergic cells (Klausberger & Somogyi, 2008) is not only gating time windows for activity, or switching on and off pyramidal cells but that the diversity of interneurons is also required for redistributing activity amongst cell types and cell compartments in a very specific manner to encode and process information content.

An emerging question addressing mechanisms underlying fear extinction learning is how activity of distinct amygdala principle neurons (PNs) is regulated. It has been shown that fear and extinction cells have specific firing patterns, which correlate with behavior (Herry et al., 2008). Furthermore, the balance between mPFC-projecting PN_{PL}s and PN_{IL}s is important for extinction learning (Senn et al., 2014). However, it is not understood, which network mechanisms control the switch of activity between these populations of cells. Possible contributors might be local GABAergic networks by regulating PN output. Thereby, different levels of asymmetry are conceivable such as absolute connectivity, synaptic strength or involvement of modulatory systems. In this scenario CCK interneurons are particularly interesting, as they have been implicated to play a role in mood disorders and fear extinction processes (Marsicano et al. 2002, Freund 2003). CCK interneurons express presynaptic CB1Rs (Mascagni & McDonald, 2003), which allow for activity dependent suppression of inhibition (Wilson & Nicoll, 2002) a possible mechanism for rapid network adaptations. Furthermore, the neuropeptide CCK is released by CCK interneurons and injections of CCK-B receptor agonists have been shown to block extinction (Chhatwal et al., 2009). Therefore, the main goal of my thesis was to investigate whether CCK interneurons provide target selective input onto PN_{PL}s and PN_{IL}s that would allow for rapid network adaptations of amygdala output.

4. AIM OF THE STUDY

In the first part of my thesis a broad approach was used to explore whether GABAergic plasticity in general can be induced by fear conditioning and (in collaboration with Yu Kasugai and Francesco Ferraguti from the Medical University of Innsbruck) whether functional changes are accompanied by ultrastructural rearrangements at inhibitory synapses in basal amygdala. Therefore, I carried out whole-cell mIPSC recordings of amygdala PNs after behavioral training to study whether fear conditioning induces changes in mIPSC charge transfer and frequency. Yu Kasugai used the freeze-fracture immunolabeling technique to investigate training-induced alterations in synaptic area and $GABA_A$ receptor density.

In a next set of experiments I studied GABAergic transmission in a cell type specific manner. I explored whether CB1R-expressing CCK interneurons (CCK_Ls) provide target-selective input onto PN_{IL}s and PN_{PL}s that could lead to a switch of activity between these two amygdala output pathways. Therefore, I recorded pairs of CCK_Ls and PN_{IL}s/PN_{PL}s in whole-cell configuration and tested potential asymmetries on the level of absolute connectivity, synaptic strength, short-term plasticity and endocannabinoid signaling. Complementary to electrophysiological experiments I used immunohistochemical stainings and confocal microscopy to underpin the findings.

5. RESULTS

5. 1. Project I - Fear conditioning induces functional and ultrastructural changes at GABAergic synapses in amygdala

Yu Kasugai[1], Elisabeth Vogel[2], Andreas Lüthi[2], Francesco Ferraguti[1*]

[1]*Dept. Pharmacol., Innsbruck Med. Univ., Innsbruck, Austria*
[2]*Friedrich Miescher Institute for Biomedical Research, Basel, Switzerland*

5. 1. 1. Abstract

Adaptive defensive behaviors such as conditioned fear responses are acquired through processes involving activity-dependent functional and structural changes in synaptic transmission. We report that the acquisition and extinction of conditioned fear memories not only depend on experience-dependent plasticity of glutamatergic synaptic transmission, but also entails reversible functional and structural remodeling of GABAergic synapses onto principal neurons in basal amygdala (BA). Fear conditioning induced an expansion of the postsynaptic area through synapse rearrangement and elimination. Fear conditioning-induced structural plasticity was associated with a modification in the subunit composition of synaptic $GABA_A$ receptors and a change in mIPSC kinetics, but without altering the intrasynaptic distribution and overall amount of $GABA_A$ receptors. Fear conditioning-induced synaptic changes were reversed by extinction training. These findings demonstrate that fear learning involves concerted structural and functional remodeling of GABAergic inhibitory synapses and suggest a role for plasticity of synaptic inhibition in orchestrating neuronal circuit activity during the formation and storage of associative fear memories.

5. 1. 2. Introduction

Long-term changes in synaptic strength and circuit refinement following associative learning have been extensively studied at excitatory glutamatergic synapses (Yuste and Bonhoeffer, 2001; Matsuzaki et al., 2004). Activity-driven structural changes include elimination and formation of synapses, actin-dependent stabilization and enlargement of the postsynaptic density as well as alteration in ionotropic glutamate receptors (Holtmaat & Svoboda 2009; Caroni et al., 2012). Plasticity at inhibitory synapses has received much less attention despite its contribution to the maintenance of the stability, the wide dynamic range and high computational flexibility of neuronal circuits (Castillo et al., 2011; Maffei, 2011). Only in recent years, altered sensory experience was shown to induce remodeling not only of spines but also of spatially clustered inhibitory synapses in the visual cortex (Chen et al., 2012).

Pavlovian fear conditioning is one of the most studied forms of associative learning that largely depends on synaptic plasticity in the amygdala (Pape and Pare, 2010). It represents an important model in the study of the neurobiology of normal and pathological fear (Graham & Milad, 2011). Generally, it is agreed that after fear conditioning pyramidal-like neurons in the basolateral amygdala (BLA), comprised of the lateral (LA) and basal (BA) nuclei, are activated by associative excitatory inputs and undergo complex synaptic changes (Herry & Johansen, 2014) including an increase in spine volume (Ostroff et al., 2010). A large body of evidence suggests that fear engrams depend also on inhibitory elements within amygdala networks (Ehrlich et al., 2009). Inhibitory GABAergic circuits are known to gate the acquisition and expression of fear memories not only by tuning excitatory transmission, but also by playing more active roles in amygdala intrinsic fear pathways (Ehrlich et al., 2009; Wolff et al., 2014). Furthermore, amygdala inhibitory circuits appear to be involved in the formation of new suppressive memories during fear extinction (Herry et al., 2010). The critical involvement of the GABAergic system in the regulation of fear is also highlighted by the fact that drugs modulating $GABA_A$ receptor channels, such as benzodiazepines (BZs), have been used for decades to treat anxiety disorders and are able to inhibit fear memory acquisition, consolidation and extinction (Makkar et al., 2010). Additionally, ex vivo studies on GABA receptor subunit expression (Heldt &

Ressler, 2007) and the regulation of GABA receptor associated proteins (Chhatwal et al., 2005) suggest that fear conditioning leads to decreased levels of inhibition whereas extinction of fear results in enhanced inhibitory transmission.

Here, we addressed whether classical fear conditioning and extinction induce functional and structural plasticity at inhibitory synapses of the BA using a combination of electrophysiological and high-resolution ultrastructural approaches in mice.

5. 1. 3. Materials and methods

5. 1. 3. 1. Animals and behavior

For electrophysiological experiments male C57BL/6 mice (RCC, Füllinsdorf, Switzerland) were used. Seven to nine week old animals were housed separately in a temperature controlled room and a 12/12 h light/dark cycle. All procedures were carried out with an approval by the Veterinary Department of the Canton Basel-Stadt.

Mice were submitted to an auditory fear-conditioning paradigm with 5 CSs (7.5 kHz, 30 x 50 ms pips, 80 dB), each preceding one US (mild foot shock, 0.6 mA, 1 s) as previously described (Herry et al., 2008). In order to deliver tone/shock pairings, a current generator and scrambler was controlled by a computer running the TruScan 99 software (Coulbourn Instruments, Allentown, PA). Fear retrieval and fear extinction training sessions were performed 24 h and 48 h after the conditioning in a new context with different visual and olfactory cues. Freezing behavior was defined as the absence of movement except respiration for at least 2 s and was quantified during each behavioral session by an automatic infrared beam detection system (Coulbourn Instruments) (Herry et al., 2008).

5. 1. 3. 2. Electrophysiology

Three hours after behavioral training, animals were anesthetized with isoflurane and decapitated as described (Bissière et al., 2003). Briefly, brains were dissected in ice-cold artificial cerebrospinal fluid (ACSF), and coronal slices (300 µm thick) were prepared at 4 ºC with a vibratome (Microm HM 650 V; Walldorf, Germany). Slices were recovered for 45 min at 37 ºC in an interface chamber containing ACSF equilibrated with 95% O_2/5% CO_2. The ACSF contained (in mM): 124 NaCl, 2.7 KCl, 2 $CaCl_2$, 1.3 $MgCl_2$, 26 $NaHCO_3$, 0.4 NaH_2PO_4, 18 glucose, 2.25 ascorbate. Neurons were visually identified with infrared video microscopy using an upright microscope equipped with x5 and x40 objectives (Olympus, Germany). Whole-cell patch-clamp recordings were obtained from projection neurons in the BA at 31-33 °C in a submerged chamber under constant superfusion with ACSF. Patch electrodes (4.5 - 5.5 MΩ) were pulled from borosilicate glass tubing and filled with an intracellular solution consisting of (in mM): 130 KCl, 10 HEPES, 10 phosphocreatineNa_2, 4 Mg-ATP, 0.4 Na-GTP (pH adjusted to 7.25 with KOH, ~ 290 – 300 mOsm). The membrane potential was held at −80 mV in voltage-clamp recordings. In order to block glutamatergic synaptic transmission all recordings were carried out in the presence of CPP (20 µM), CNQX (20 µM) and TTX (1 µM). Data were acquired with pClamp9 (Molecular Devices) and recorded with a Multiclamp 700A amplifier (Molecular Devices). Data were sampled at 20 kHz and filtered at 2 kHz. Series resistance was monitored every 3 min by applying a –5 mV hyperpolarizing pulse. If during an experiment series resistance changed more than 20%, or exceeded 20 MΩ, recordings were discarded. mIPSC recordings were achieved in the gap-free modus. For each neuron, at least 276 mIPSC events were recorded. Frequency, amplitude, charge transfer and kinetics of mIPSCs were analyzed offline using the Mini Analysis Program (version 6.0.9, Synaptosoft). The threshold for mIPSC detection was set to 27 pA. All values are expressed as means ± s.e.m. Statistical comparisons were done with a one-way ANOVA followed by a post-hoc Bonferroni test corrected for multiple comparisons (as appropriate two-tailed $p < 0.05$ was considered significant).

5. 1. 3. 3. Freeze fracture immunelabeling

FRIL was performed according to previously published procedures (Kaufmann et al., 2013). Brains of animals (male C57BL/6 mice) were perfused with PB (0.1 M, pH 7.4) containing 1% formaldehyde and 15% of a saturated solution of picric acid. Forebrains were cut into 140 µm thick coronal sections with a Vibratome (Leica Microsystems VT1000S), cryoprotected overnight with 30% glycerol and then frozen by use of a high-pressure freezing machine (HPM 010; Bal-Tec, Balzers, Liechtenstein). Using a double replica method frozen specimens were fractured by a freeze-etching device (BAF 060; Bal-Tec) at -115° C. Fractured faces were replicated by evaporation of carbon (rotating) by means of an electron beam gun positioned at a 90° angle to a thickness of 5 nm and shadowed unidirectionally with platinum-carbon at a 60° angle (thickness 2 nm). Finally, an additional 15 nm thick layer of carbon was applied. Tissue was solubilized in a solution containing 2.5% sodium lauryl sulfate (SDS) and 20% sucrose in 15 mM Tris buffer, pH 8.3, on a shaking platform for 18 hours at 80°C. Replicas were kept in the same solution at RT until processed further.

On the day of immunolabeling, replicas were preincubated in a blocking solution containing 5% BSA in TBS for 1 h at RT, and then incubated in the primary antibody diluted in TBS containing 2% BSA and 2% NGS, overnight at 6°C. After several washing steps in TBS, replicas were reacted with gold-conjugated secondary antibodies overnight at 6°C. They were subsequently washed in MilliQ water, mounted on formvar-coated 100-line copper grids and analyzed in a Philips CM120 TEM equipped with a Morada CCD camera (Soft Imaging Systems). Whole images were level adjusted, sharpened, and cropped in Photoshop (Adobe) without changing any specific features. Somatic and dendritic GABAergic synapses were randomly selected. Both complete and partial synapses were analyzed. Synapses are often partially masked by other membrane leaflets. Masked synapses were referred to as partial synapses.

All locations of the gold particles in the synaptic area were marked in the virtual synapse to make a heat map with ImageJ 1.45s (NIH, USA) The area

of virtual synapse was divided into 3 fields, “Inner”, “Inner middle” and “Outer middle”, and the ratios of gold particle in each field were compared.

5. 1. 4. Results

5. 1. 4. 1. Fear conditioning increases mIPSC charge transfer and frequency in basal amygdala

To examine possible functional changes induced by fear conditioning and extinction, we measured miniature inhibitory postsynaptic currents (mIPSCs) using whole-cell patch-clamp recordings from BA principal neurons (*n* = 111) in acute brain slices. When comparing recordings obtained in slices from control animals exposed to the CS only with recordings in slices prepared after animals were subjected to fear conditioning or fear extinction training, we found no significant changes in mIPSC amplitude (Figure 6C, D). However, the amount of charge conducted per individual mIPSC (mIPSC charge transfer) was significantly enhanced when tested 3 h and 24 h after fear conditioning, but not after fear extinction (Figure 6C, D). This increase in mIPSC charge transfer could be accounted for by changes in mIPSC kinetics. Compared to CS only control animals, fear conditioning induced an increase in mIPSC 10-90% rise time and mIPSC decay time constant (Figure 6C, D). Further, mIPSC frequency was increased 24 h after fear conditioning (Figure 6C, D).

Taken together, we found that fear conditioning induced changes in mIPSC kinetics causing an increased inhibitory charge transfer per mIPSC. Moreover, changes in mIPSC frequency may indicate that fear conditioning increases the number of inhibitory synapses onto BA principal neurons.

In contrast to these observations in basal amygdala, fear conditioning or extinction did not induce changes in mIPSCs of principal neurons located in lateral amygdala (*n* = 109) (Fig 7).

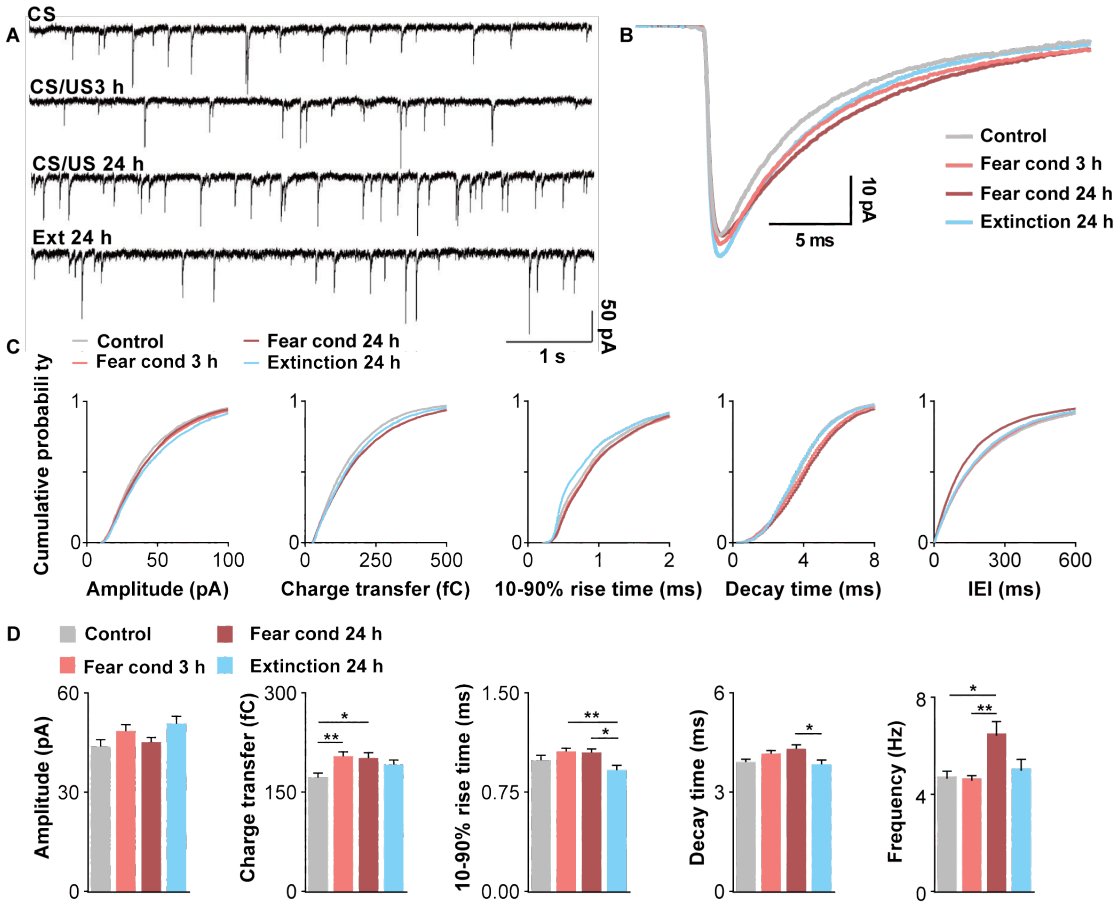

Figure 6. Fear conditioning increases mIPSC charge transfer and frequency. (**A**) Example traces illustrating a 6.5 s sweep of mIPSCs recorded from different behavioral groups. (**B**) Examples of averaged mIPSC traces illustrating fear conditioning and extinction induced changes in mIPSC kinetics. Traces were obtained by averaging all mIPSCs recorded from one representative cell (CS: *n* = 1399 mIPSCs; CS/US 3 h: *n* = 594; CS/US 24 h: *n* = 734; Ext 24 h: *n* = 1143). (**C**) Cumulative plots comparing mIPSC properties between different behavioral groups. To construct cumulative plots, 6671 events were randomly selected from each neuron and pooled. (**D**) Bar graphs illustrating fear conditioning and extinction induced changes in mIPSC kinetics and charge transfer. (*n* = 111) mIPSC amplitude (Control group: 44.07 ± 2.02 pA, *n* = 27; Fear condition 3 h group: 48.71 ± 2.09 pA, *n* = 31; Fear condition 24 h group: 45.34 ± 1.46 pA, *n* = 27; Extinction 24 h group: 50.92 ± 2.25 pA, *n* = 26; One-way ANOVA: $F_{3,107}$ = 2.56, n.s.) charge transfer (CS: 173.03 ± 6.77 fC, *n* = 27; CS/US 3 h: 205.09 ± 6.74 fC, *n* = 31; CS/US 24 h: 202.61 ± 7.95 fC, *n* = 27; Ext 24 h: 192.88 ± 6.65 fC, *n* = 26; One-way ANOVA: $F_{3,107}$ = 4.28, $p < 0.01$; Post-hoc Bonferroni multiple comparisons: CS vs. CS/US 3 h: $p < 0.01$; CS vs. CS/US 24 h: $p < 0.05$; CS only vs. Ext 24 h: n.s.; CS/US 3 h vs. CS/US 24 h: n.s.; CS/US 3 h vs. Ext. 24 h: n.s.; CS/US 24 h vs. Ext 24 h: n.s.) rise time (CS: 1.64 ± 0.04 ms, *n* = 27; CS/US 3 h: 1.74 ± 0.04 ms, *n* = 31; CS/US 24 h: 1.72 ± 0.03 ms, *n* = 27; Ext 24 h: 1.56 ± 0.04 ms, *n* = 26; One-way ANOVA: $F_{3,107}$ = 4.41, $p < 0.01$; Post-hoc Bonferroni multiple comparisons: CS vs. CS/US 3 h: n.s.; CS vs. CS/US 24 h: n.s.; CS vs. Ext 24 h: n.s.; CS/US 3 h vs. CS/US 24 h: n.s.; CS/US 3 h vs. Ext. 24 h: $p < 0.01$; CS/US 24 h vs. Ext. 24 h: $p < 0.05$) decay (CS: 3.39 ± 0.09 ms, *n* = 27; CS/US 24 h: 4.33 ± 0.12 ms, *n* = 27; Ext 24 h: 3.86 ± 0.13 ms, *n* = 26; One-way ANOVA: $F_{3,107}$ = 4.04, $p < 0.01$; Post-hoc Bonferroni multiple comparisons: CS vs. CS/US 3 h: n.s.; CS vs. CS/US 24 h: n.s.; CS vs. Ext 24 h: n.s.; CS/US 3 h vs. CS/US 24 h: n.s.; CS/US 3 h vs. Ext. 24 h: n.s.; CS/US 24 h vs. Ext 24 h: $p < 0.05$) and mIPSC frequency (CS: 4.76 ± 0.32 Hz, *n* = 27 cells; CS/US 3 h: 4.68 ± 0.23 Hz, *n* = 31; CS/US 24 h: 6.54 ± 0.59 Hz, *n* = 27; One-way ANOVA: $F_{3,107}$ = 4.56, $p < 0.01$, Post-hoc Bonferroni multiple comparisons: CS vs. CS/US 3 h: n.s.; CS vs. CS/US 24 h: $p < 0.05$; CS vs. Ext 24h: n.s.; CS/US 3 h vs. CS/US 24 h: $p < 0.01$; CS/US 3 h vs. Ext. 24 h: n.s.; CS/US 24 h vs. Ext 24 h: n.s.) Data are shown as mean ± s.e.m.; *$p < 0.05$, **$p < 0.01$.

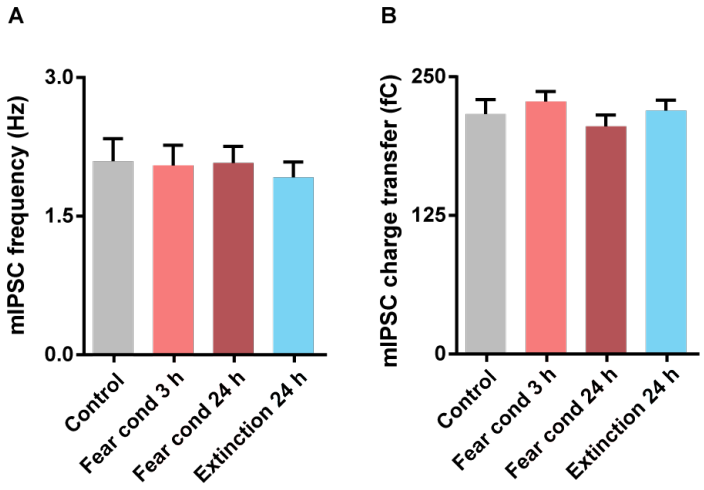

Figure 7. Fear conditioning has no effect on mIPSC recorded in lateral amygdala. (**A**) Bar graphs illustrating mIPSC frequency and charge transfer in LA neurons of control groups, fear conditioned and extinguished mice (n=109). mIPSC frequency (Control group: 2.09 ± 0.25 Hz, *n* = 28; Fear condition 3 h group: 2.05 ± 0.22 Hz, *n* = 28; Fear condition 24 h group: 2.06 ± 0.18 Hz, *n* = 25; Extinction 24 h group: 1.92 ± 0.17 Hz, *n* = 28; One-way ANOVA: $F_{3,\ 105}$ = 0.1493, n.s.) charge transfer (Control group: 216.5 ± 13.02 fC, *n* = 28; Fear condition 3 h group: 227.6 ± 9.28 fC, *n* = 28; Fear condition 24 h group: 205.2 ± 10.31 fC, *n* = 25; Extinction 24 h group: 219.5 ± 9.33 fC, *n* = 28; One-way ANOVA: $F_{3,\ 105}$ = 0.7332, n.s.)

5. 1. 4. 2. Fear conditioning induces structural plasticity at GABAergic synapses

In collaboration with the Ferraguti lab in Innsbruck it was investigated whether this increase in mIPSC charge transfer and frequency after fear conditioning was accompanied by structural changes at GABAergic synapses. Therefore the detergent-solubilized freeze-fracture replica immunolabeling (FRIL) method was used. This approach allowed examining possible changes in synaptic morphology and density of $GABA_A$ receptors in the basal amygdaloid nucleus (BA). FRIL gives a planar view of the postsynaptic specialization of GABAergic synapses detectable as a cluster of intramembrane particles (IMPs) at the protoplasmic (P)-face of replica (Figure 8A-C), which can be labeled for $GABA_A$ receptor subunits or neuroligin 2 (Kasugai et al., 2010). To selectively detect GABAergic synapses containing BZ-sensitive $GABA_A$ receptors, highly specific γ2 subunit antibodies were used.

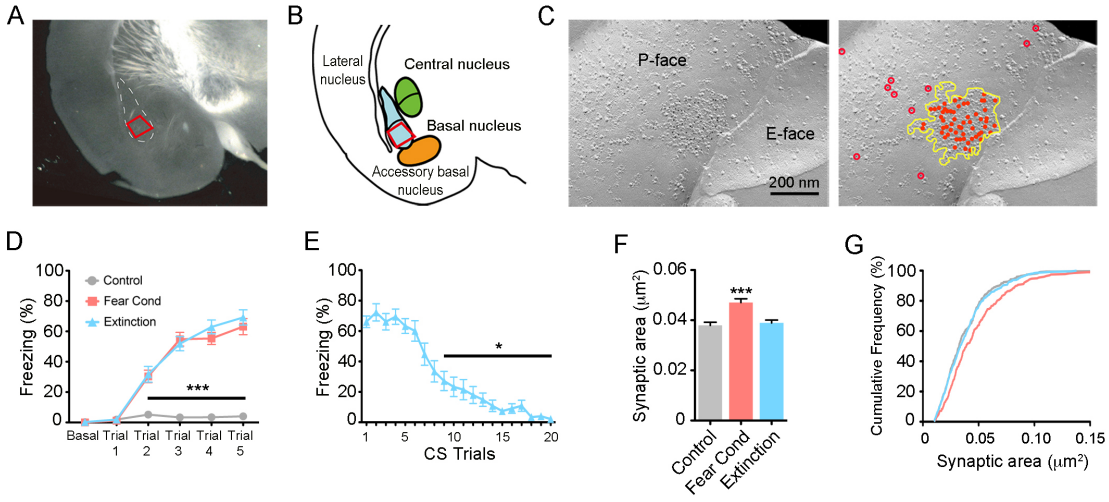

Figure 8. Fear and extinction-mediated bi-directional structural adaptation of GABAergic synapses. (**A**) Coronal section and (**B**) diagram of the amygdala showing the area (in red) dissected out for FRIL. (**C**) Electron-micrograph of a dendrite of a pyramidal-like neuron in the BA. The postsynaptic density of a GABAergic synapse is visible as a cluster of intramembrane particles (area outlined in yellow) on the protoplasmic face of the replica, which is immunolabelled with 5nm gold particles identifying the γ_2-subunit of $GABA_A$ receptors. Gold particles are highlighted (right panel) by solid red dots when intrasynaptic and red circles when extrasynaptic. (**D**) Freezing responses of the paired (fear conditioned and extinction groups, 5 pairings, 0.7 mA foot shock) and control (exposed to the conditioned stimulus only) groups (n = 10 for each group). (**E**) Extinction training. Data were analyzed by One-way ANOVA followed by *posthoc* Bonferroni (* $p < 0.05$, *** $p < 0.001$). (**F**) In fear conditioned mice the GABA-PSA (0.047 ± 0.001 μm^2, n = 396) was significantly larger (Kruskal-Wallis test followed by *posthoc* Dunn's multiple comparisons) when compared to the control (*** $p < 0.001$, 0.038 ± 0.001 μm^2, n = 344) and extinction (*** $p < 0.001$, 0.039 ± 0.023 μm2, n = 432) groups. The synaptic area was determined only for full synapses. Synapses were collected from 4 animals/group and 2 replica/mouse. As there was no significant difference among animals in each group (Kruskal-Wallis test, control $p > 0.05$, fear conditioning $p > 0.05$, extinction $p > 0.05$), data were pooled. (**G**) Cumulative frequency distribution of the postsynaptic area of GABAergic synapses. Cumulative frequency distribution data were analyzed by means of the two-sample Kolmogorov–Smirnov test: control vs. fear conditioning $p < 0.001$; extinction vs. fear conditioning $p < 0.001$. Data are shown as mean ± s.e.m..

First, it was investigated whether fear conditioning affects the postsynaptic area of GABAergic synapses (GABA-PSA) and the density of $GABA_A$ receptors containing the γ_2-subunit in BA neurons. Mice were randomly assigned to 3 groups. Two of the groups (fear conditioning and extinction) were subjected 5 times to a neutral auditory cue paired with a co-terminating foot shock, whereas the third group (control) was exposed only to the tone in the conditioning chamber. Fear conditioned mice, but not the control group, showed robust freezing responses (Figure 8D). Twenty-four hours after fear

conditioning, mice in the extinction group exhibited a selective increase in fear behavior when exposed to the tone in a different context. Extinction of conditioned fear was then induced by exposing the mice to 20 tone presentations in the absence of the foot shock that resulted at the end of the extinction training in levels of freezing similar to pre-conditioning (Figure 8E). After behavioral testing, mice were returned to their home cages and two hours later processed for FRIL. After fixation of the brain and coronal sectioning, specimens from the BA were carefully dissected out under a stereomicroscope, high pressure frozen, fractured and replicated (Figure 8A-C). For the estimation of the synaptic area only complete GABAergic synapses immunolabelled for $GABA_A$-γ_2 were sampled from both somatic and dendritic compartments (Figure 8C). In fear conditioned mice the GABA-PSA was found significantly larger than in the control and extinction groups (Figure 8F). Because of the large variability in GABA-PSA (e.g. ranging from 0.010 to 0.153 μm^2 in control animals), cumulative frequency distributions were also analyzed (Figure 8G). A significant shift towards a higher frequency of synapses with larger area was observed in fear conditioned mice.

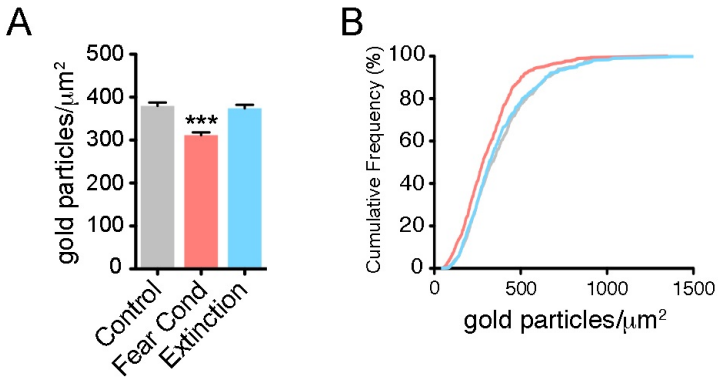

Figure 9. Fear learning induces a decrease in $GABA_A$-γ_2 synaptic density.
(**A**) $GABA_A$-γ_2 synaptic density was significantly reduced after fear conditioning, but fully recovered after extinction (Kruskal-Wallis test followed by Dunn's multiple comparisons; *** $p < 0.001$ control vs. fear conditioning; *** $p < 0.001$ extinction vs. fear conditioning). For density measures also partial synapses were analyzed (control, n = 722, 380 ± 8 particles/μm^2; fear conditioned, n = 672, 311 ± 7 particles/μm^2; extinction, n = 718, 374 ± 2 particles/μm^2). (**B**) Cumulative frequency distribution of the $GABA_A$-γ_2 synaptic density. Cumulative frequency distribution data were analyzed by means of the two-sample Kolmogorov–Smirnov test: control vs. fear conditioning $p < 0.001$; extinction vs. fear conditioning $p < 0.001$. Data are shown as mean ± s.e.m..

Next, we measured the synaptic density of gold particles for $GABA_A$-γ_2 at replica P-face. For this analysis both complete and partial synapses were included. Fear conditioned mice showed a significant reduction of the mean $GABA_A$-γ_2 synaptic labeling density compared to the control and extinction groups (Figure 9A). Cumulative frequency distributions also revealed a significant shift of the synaptic γ_2 labeling density in fear conditioned mice (Figure 9B).

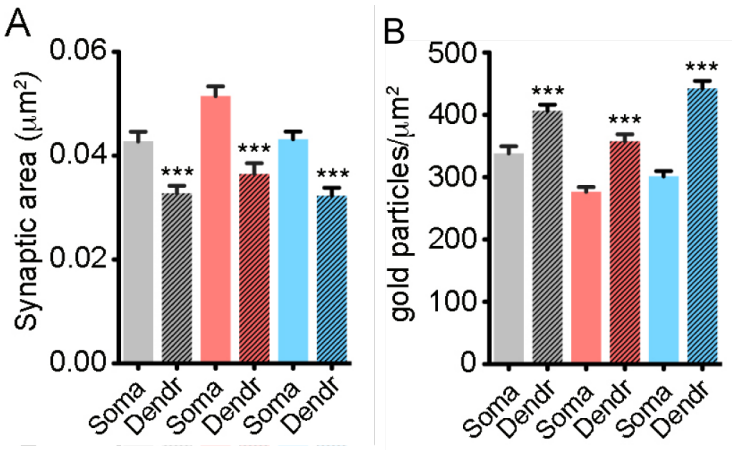

Figure 10. Fear and extinction influence both perisomatic and dendritic synapses. (**A**) Fear conditioning- and extinction-mediated remodeling of GABA-PSA occurs at both perisomatic and dendritic synapses. Perisomatic BZ-sensitive GABAergic synapses are larger than dendritic synapses in the control, fear conditioning (soma 0.043 ± 0.002 μm^2, *n* = 179; dendrites 0.033 ± 0.001 μm^2, *n* = 165; *** $p < 0.001$), and extinction groups. (**B**) Perisomatic GABAergic synapses possess a lower density of BZ-sensitive $GABA_A$ receptors compared to dendritic ones. Reduced synaptic $GABA_A$-γ_2 density after fear conditioning was observed in both perisomatic (338 ± 11 particles/μm^2, *n* = 283) and dendritic synapses (406 ± 10 particles/μm^2, *n* = 439) *** $p < 0.001$ Data are shown as mean ± s.e.m..

Changes in GABA-PSA and density of $GABA_A$ receptors containing the γ_2-subunit after fear conditioning were found to take place in both perisomatic as well as dendritic synapses (Figure 10). Remarkably, we found that dendritic synapses possessed a higher density of $GABA_A$ receptors compared to perisomatic ones, whereas as expected the average area of the latter synapses (0.043 ± 0.002 μm^2) was larger than those on dendrites (0.033 ± 0.001 μm^2). Also for perisomatic and dendritic synapses extinction was able to fully reverse fear-mediated structural changes (Figure 10).

These results indicate that fear-mediated structural plasticity occurs at both somatic and dendritic GABAergic synapses, and that it involves multiple types of interneurons targeting different subcellular domains of BA pyramidal neurons.

5. 1. 4. 3. Fear conditioning-induced structural plasticity is long lasting

To ensure that the extinction-induced reversal of the GABA-PSA remodeling and $GABA_A$-γ_2 synaptic labeling density was mediated by extinction training rather than time-lapse, in a separate set of experiments we measured these parameters 26 h after conditioning, equivalent to the extinction protocol (Figure 11A). Consistent with the notion that the fear extinction-induced reversal is an active process induced by extinction learning, we found that 26 h after fear conditioning the mean GABA-PSA was still larger and its cumulative frequency distribution significantly right shifted compared to control mice (Figure 11B). Likewise, the $GABA_A$-γ_2 synaptic labeling density and the corresponding cumulative frequency distribution remained significantly altered compared to control mice (Figure 11C).

Our data thus indicate that fear conditioning-induced plasticity is long lasting (> 24 hours) and associated to fear memory consolidation. Furthermore, it suggests that extinction training indeed mediates the reversal of synaptic structural plasticity induced by fear conditioning.

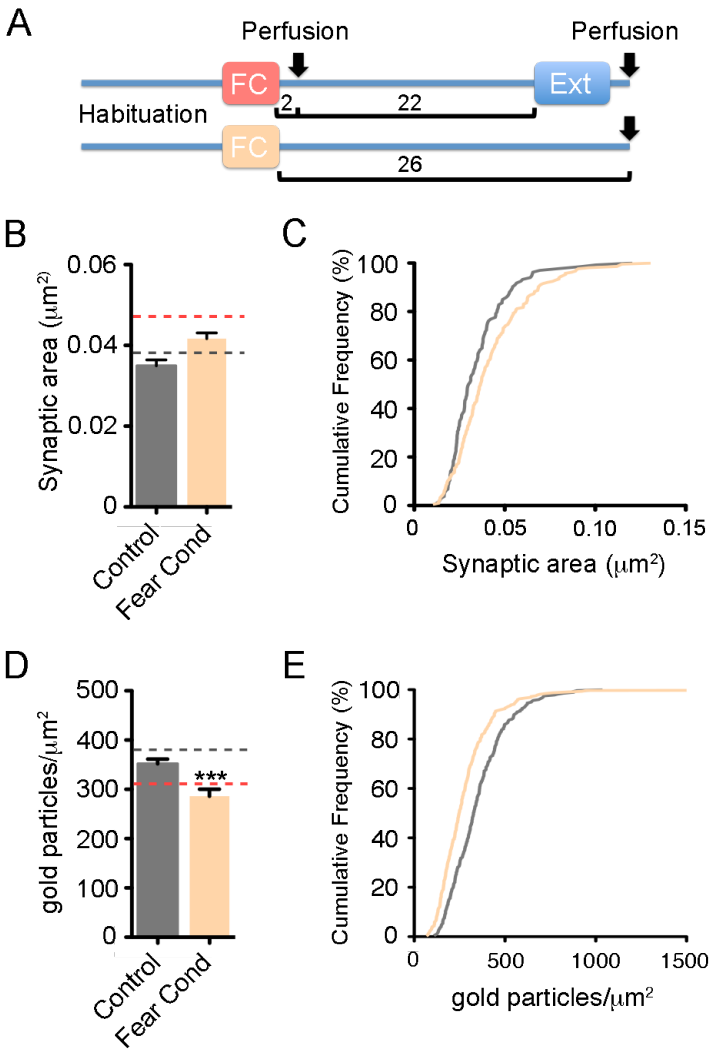

Figure 11. Fear learning induces long lasting structural plasticity. (**A**) Schematic diagram of the experimental design. (**B**) After 26 h from fear conditioning the mean GABA-PSA (0.042 ± 0.021 μm^2, *n* = 213 synapses) was still significantly larger (Mann Whitney, ** p < 0.01) compared to the control group (0.035 ± 0.017 μm^2, synapses *n* = 135). The synaptic area was determined only for full synapses. Synapses were collected from 3 animals/group and 2 replicas/mouse. As there was no significant difference among animals in each group (Kruskal-Wallis test), data were pooled. Dashed lines indicate values from fear cond 3 h group and corresponding controls. (**C**) Cumulative frequency plot of the postsynaptic area of GABAergic synapses 26 h after fear conditioning or CS-alone (control). Two sample Kolmogorov-Smirnov test, $p < 0.05$) (**D**) $GABA_A$-γ_2 synaptic density was also reduced 26 h after fear conditioning (Mann Whitney, *** $p < 0.01$). For density measures also partial synapses were analyzed (Fear conditioning, 286 ± 250 particles/μm^2, *n* = 324; Control group 351 ± 157 particles/μm^2, *n* = 277). Dashed lines indicate values from fear cond 3 h group and corresponding controls. (**E**) Cumulative frequency plot of the $GABA_A$-γ_2 synaptic density 26 h after fear conditioning or CS-alone (control). Cumulative frequency distribution data were analyzed by means of the two-sample Kolmogorov–Smirnov test. Data are shown as mean ± s.e.m..

5. 1. 4. 4. Fear conditioning increases the ratio of synaptic $GABA_A$ receptors containing the α_2 subunit

Because of the changes in mIPSC kinetics, we hypothesized a shift in the subunit composition of synaptic $GABA_A$ receptors following fear conditioning, as $GABA_A$ receptors composed of different α-subunits display diverse gating kinetics (Eyre et al., 2012; Geracitano et al., 2012). Using the FRIL technique on replica obtained from the very same animals analyzed for $GABA_A$-γ_2, we examined the GABA-PSA and density of $GABA_A$ receptors containing the α_2 subunit, which may be involved in mediating anxiolytic properties of benzodiazepines (Rudolph & Möhler, 2004), in BA neurons (Figure 12A). A highly significant increase in the mean GABA-PSA and shift in the cumulative frequency distribution towards synapses with larger area were confirmed in the fear-conditioned group when compared to the control group (Figure 12B). Extinction training once again restored the GABA-PSA to control levels (Figure 12B). Conversely, no significant differences in the density of the synaptic $GABA_A$-α_2 subunit were detected among the 3 groups ($p = 0.93$). These findings indicate that fear conditioning increases the ratio of synaptic $GABA_A$ receptors containing the α_2 subunit.

In conclusion, our results indicate that fear and extinction learning induced experience-dependent, reversible, structural and functional changes at GABAergic synapse onto BA principal neurons. These changes may serve to the maintenance and the stability of the dynamic range of neuronal circuit activity in relation to complex adaptive behaviors such as conditioned fear, and could contribute to metaplasticity.

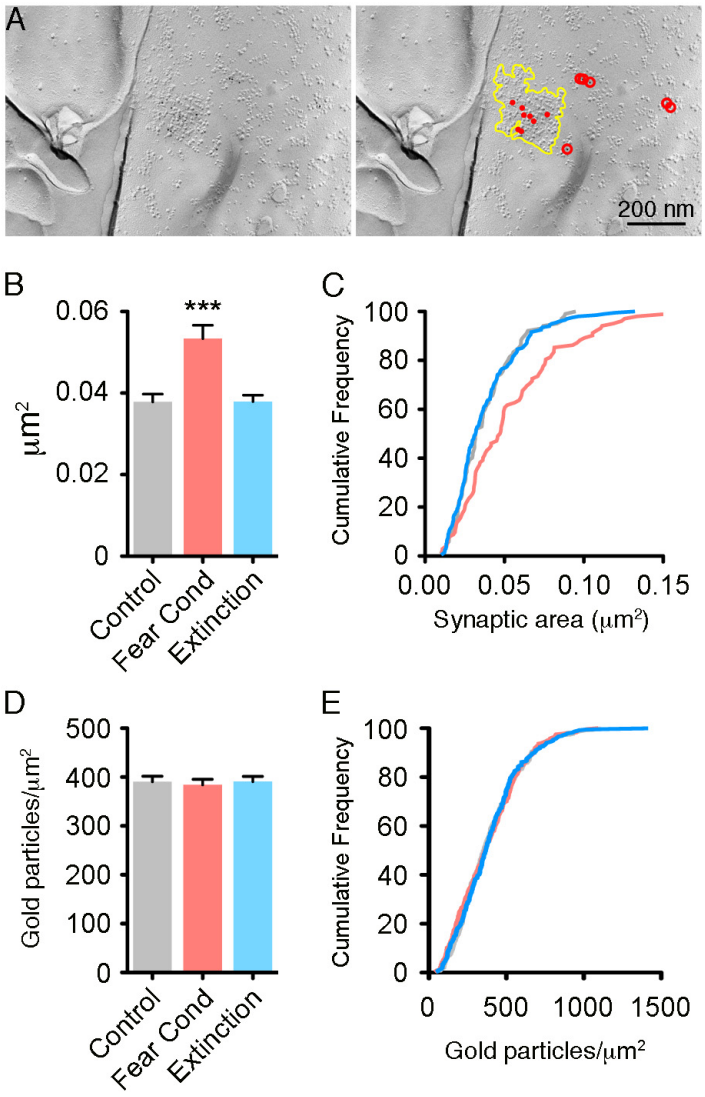

Figure 12. Fear mediates a subunit composition change in synaptic $GABA_A$ receptors. (**A**) GABAergic synapses containing $GABA_A$-α_2 receptors had a larger mean area in fear conditioned mice compared to both control and extinction animals (Dunn's multiple comparison test, *** $p < 0.001$). The synaptic area was determined only for full synapses. Synapses were collected from 4 animals/group and 2 replicas/mouse. As there was no significant difference among animals in each group (Kruskal-Wallis test), data were pooled (synapses: control, $n = 102$; fear conditioned, $n = 102$; extinction, $n = 201$). (**B**) Cumulative frequency distribution of the postsynaptic area of GABAergic synapses. (**C**) Cumulative frequency distribution of the $GABA_A$-α_2 synaptic density; the right shift of the fear conditioned group was even more prominent than for synapses labeled for the $GABA_A$-γ_2. The mean of α_2-positive GABA-PSA in fear conditioned mice (mean ± SEM, 0.053 ± 0.003 μm^2, $n = 102$) was significantly larger (Mann Whitney test, $p < 0.0001$) compared to the control (0.038 ± 0.002 μm^2, $n = 102$) group, and it returned to the control level in the extinction group (0.038 ± 0.002 μm^2, $n = 201$. (**D**) $GABA_A$-α_2 synaptic density was similar among the 3 groups suggesting an increased ratio of synaptic $GABA_A$ receptors containing α_2 subunits as a consequence of fear conditioning. For density measures also partial synapses were analyzed (control $n = 348$; fear conditioned $n = 364$; extinction $n = 390$).

5. 1. 5. Discussion

Our data demonstrate that bi-directional morphological alterations at BA inhibitory synapses induced by fear conditioning and extinction are paralleled by reversible functional changes in synaptic physiology. Overall, it is indicated that fear conditioning promotes a strengthening of GABAergic transmission which is reversed by fear extinction. These results are the first example of learning induced structural and functional plasticity at inhibitory synapses.
Data suggest that fear conditioning induced an enlargement of GABAergic synapses. Previously, it has been shown that LTP leads to an overall increase in size of excitatory synapses by elimination of small spines at hippocampal dendrites. In parallel, the same LTP protocol increased the synaptic surface area at inhibitory synapses while the absolute number of synapses was reduced (Bourne & Harris, 2011). Thus, one possible explanation for the mean enlargement of GABAergic synapses induced by fear conditioning may be the elimination of small synapses. Moreover, data indicate that behavioral training reduces the $GABA_A$-γ_2 synaptic density but, as the synaptic area is enlarged, has no effect on the number of receptors. Considering the observed rearrangements in receptor subunit composition, another explanation for an enlargement of synaptic area may involve a structural remodeling of the synapse.

The recorded increase in mIPSC charge transfer was rather due to changes in kinetics than in amplitude. It has been shown that $GABA_A$ receptors composed of different α-subunits display diverse gating kinetics (Eyre et al., 2012; Geracitano et al., 2012). Therefore, a rearrangement in $GABA_A$ receptor subunit composition may underlie slower kinetics and higher charge transfer which overall lead to a strengthening of synaptic transmission. However, it cannot be excluded that structural and functional changes reflect independent mechanisms.
In contrast to previous findings (Heldt & Ressler, 2007; Chhatwal et al., 2005), we demonstrated that fear learning was not associated with a decrease in synaptic inhibition, but an increase in mIPSC charge transfer and synaptic

size. It is reasonable that a lower expression of $GABA_A$ receptor subunit α_1 after conditioning (Heldt & Ressler, 2007) is associated and in line with our findings that show an increase in subunit α_2. Also, decreased levels of gephyrin mRNA after fear conditioning (Chhatwal et al., 2005) could be explained by a remodeling of the synapse.

Generally, enhanced inhibitory transmission might be important for maintaining the balance between excitation and inhibition. However, the observed strengthening of inhibitory synapses might only reflect a net effect whereas input onto different cell types such as fear or extinction neurons (Herry et al., 2008) could be regulated antagonistically during high fear and low fear states.
In lateral amygdala fear conditioning and extinction did not induce any changes in mIPSC properties. It is generally believed that the LA is the site of CS and US convergence and it has been shown that lesions of the LA lead to an impairment of auditory fear conditioning (LeDoux et al., 1990). Moreover, fear conditioning induces a potentiation of excitatory currents onto LA pyramidal cells (MCKernan & Shinnick-Gallagher, 1997). Therefore, it is surprising, that fear learning did not lead to changes in inhibitory transmission. However, it cannot be excluded that subtype specific effects in opposite directions might occur or that induced changes are not detectable by mIPSC recordings in unidentified cells.

Basal amygdala interneurons are represented by a large variety of cell types, with different activity patterns, molecular marker expression and targeting of postsynaptic subdomains. Whole cell patch clamp recordings of mIPSCs might be dominated by somatically targeting interneurons, however, structural plasticity occurs at dendritic and somatic synapses, suggesting that multiple types of interneurons are involved.

5. 1. 6. Author contributions

Y.K. performed FRIL experiments. E.V. carried out electrophysiological recordings. Y.K., E.V., A.L. and F.F. wrote the paper.

5. 2. Project II - Projection-specific dynamic regulation of inhibition in amygdala micro-circuits

Elisabeth Vogel[1,2], Sabine Krabbe[1], Jan Gründemann[1], Jaclyn I. Wamsteeker Cusulin[1], Andreas Lüthi[1]

[1]Friedrich Miescher Institute for Biomedical Research, Basel, Switzerland.
[2]University of Basel, Basel, Switzerland.

5. 2. 1. Abstract

Cannabinoid receptor type 1 (CB1R) expressing CCK interneurons are major regulators of cortical circuits. Here we report that retrograde endocannabinoid signaling and CB1R-mediated regulation of inhibitory synaptic transmission onto basal amygdala principal neurons strongly depend on principal neuron projection target. Projection-specific asymmetries in the regulation of local inhibitory micro-circuits may contribute to the selective activation of distinct amygdala output pathways during behavioral changes.

5. 2. 2. Introduction

Principal neurons (PNs) in cortex-like structures are heterogeneous populations of cells, which can be functionally distinct but anatomically intermingled (Le Be and Markram, 2006; Brown and Hestrin, 2009; Senn et al., 2014). Their long-range axonal projection target often defines their identity and the probability of local connectivity within glutamatergic circuits (Le Be and Markram, 2006; Brown and Hestrin, 2009). Given that PN activity is tightly controlled by local inhibitory circuits, this raises the question whether local inhibition is also organized in a cell-type specific manner. Data from many cortical areas indicate that inhibitory control within local microcircuits is typically broad (Wehr and Zador, 2003; Liu et al., 2010; Bock et al., 2011; Hofer et al., 2011; Harris and Mrsic-Flogel, 2013). However, recent work revealed that cholecystokinin (CCK) and type 1 cannabinoid receptor (CB1R) expressing interneurons (CCK INs) in entorhinal cortex differentially inhibit distinct populations of PNs, suggesting that local inhibitory circuits mediated

by specific IN subtypes may contribute to the regulation and selection of defined output pathways (Varga et al., 2010).

From the basal nucleus of the amygdala (BA), distinct populations of PNs project to the prelimbic (PL) or infralimbic (IL) subdivisions of the medial prefrontal cortex (mPFC) (LeDoux, 2000). Basal amygdala PL-projecting PNs (PN_{PL}s) are activated *in vivo* during states of high fear, whereas IL-projecting PNs (PN_{IL}s) increase their activity in low fear states, such as with acquisition of extinction, which is consistent with the function of the targeted mPFC subdivisions (Quirk and Mueller, 2008; Burgos-Robles et al., 2009; Sierra-Mercado et al., 2011). Recent data indicate that the switch between high fear and low fear states is mediated by a shift of activity in these two amygdala output pathways (Senn et al., 2014). However, the underlying circuit mechanisms mediating such a shift remain unknown.

CB1R expressing CCK INs have been suggested to play an important role in mood disorders and fear extinction processes (Marsicano et al., 2002, Freund, 2003). In the amygdala, large-somata CCK INs (CCK_Ls) represent the sole amygdala IN type expressing CB1Rs and form a population distinct from calretinin and/or vasoactive intestinal peptide (VIP)-expressing small CCK INs (CCK_Ss) (Mascagni and McDonald, 2003). Given the necessity of amygdala CB1Rs and endocannabinoids in fear extinction (Marsicano et al., 2002) and opposing behavioral functions of projections from the BA to the PL or IL during fear extinction, we tested the hypothesis that local BA CCK_Ls differentially inhibit defined subpopulations of BA PNs to balance the activity of functionally distinct BA→mPFC output pathways.

5. 2. 3. Materials and Methods

5. 2. 3. 1. Animals

Mice were group housed in a temperature-controlled room with a 12 h light/dark cycle and unlimited access to food and water. All procedures were carried out with the approval of the Veterinary Department of the Canton Basel-Stadt.

CCK-IN-GFP transgenic mice were generated using an intersectional strategy. Mice expressing Flp under a pan-GABAergic promoter Dlx (*Dlx-Flp*) (Miyoshi et al., 2010) were crossed with *CCK-IRES-Cre* Cre-driver mice (Taniguchi et al., 2011). Subsequent crossing of *Dlx-Flp::CCK-IRES-Cre* offspring with the *RCE:dual* conditional reporter line (Taniguchi et al., 2011) yielded progeny with exclusive GFP expression in Cre^+/Flp^+ GABAergic, but not Cre^+/Flp^- glutamatergic CCK-expressing neurons (Taniguchi et al., 2011). 4-6 weeks old CCK-IN-GFP male mice were used for all experiments. Age-matched WT littermates were used for histology. Mice were single housed after surgical procedures.

5. 2. 3. 2. Stereotactic delivery of retrograde labels

Retrograde labeling of BA→mPFC projecting neurons was carried out by IL/PL localized stereotactic injections of either red fluorophore-coated latex hemispheres (Lumafluor) for electrophysiology or Alexa 555-conjugated Choleratoxin-B (Life Technologies) for histology. Beads were dialyzed against 0.32 M sucrose solution on floating polycarbonate membrane filters (Steriltech; pore size 0.01 μm, diameter 25 mm). Mice were anaesthetized with isoflurane (Minirad) in oxygen-enriched air (Oxymat 3, Weinmann) and placed in a stereotaxic frame (Kopf Instruments). Body temperature was maintained at 35.5 °C with a feedback controlled heating pad (FHC). Analgetics (meloxicam (60 μl of 0.5 mg/ml^{-1}, i.p., Metacam, Boehringer Ingelheim), ropivacain (120 μl under the scalp, Naropin, AstraZeneca)) were delivered prior to surgical incision. A picospritzer (Parker Hannifin Coorporation) connected to a flame-pulled (P-97, Sutter Instruments) borosilicate micropipette (World Precision Instruments) was used to deliver retrobeads (0.1 μl) or Choleratoxin-B (0.5 μl) bilaterally to either mPFC subdivision using the following coordinates (in mm from bregma): rostral + 1.85, lateral ± 0.35, ventral 2.2 (PL) or 2.75 (IL). Post-surgery treatment involved injection of meloxicam (60 μl of 0.5 mg/ml^{-1}, IP, Metacam) to reduce pain and inflammation risk. Animals were allowed to recover 2-7 days before subsequent experiments.

5. 2. 3. 3. Electrophysiology

Mice were deeply anaesthetized with 5 % isoflurane and decapitated. Brains were dissected in ice-cold artificial cerebrospinal fluid (aCSF) containing (in mM) 124 NaCl, 2.7 KCl, 2 $CaCl_2$, 1.3 $MgCl_2$, 26 $NaHCO_3$, 0.4 NaH_2PO_4, 18 glucose and 2.25 ascorbate, equilibrated with 95 % O_2 / 5 % CO_2. Coronal slices (300 μm thickness) were cut with a vibratome (Microm HM 650 V) with sapphire blades (Delaware Diamond Knives), stored in an interface chamber and recovered for 45 min at 37 °C. Whole-cell patch clamp recordings from CCK INs and IL/PL-projecting PN pairs/triples (max. 350 μm apart) were carried out at 32 °C under constant perfusion with 95 % O_2 / 5 % CO_2 equilibrated aCSF. GFP^+ and bead-labeled neurons were identified under an upright microscope (Olympus Model BX61) fitted with epifluoresence and infrared optics (EM-CCD Camera, Hamamatsu). Borosilicate glass (GC150T-7.5, Harvard Apparatus) was used to pull patch electrodes (DMC Universal Puller, Zeitz Instruments GmbH) with a resistance of 3-4 MΩ. Intracellular recording solution contained (in mM): 106 K-Methylsulfate, 40 KCl, 20 Na-Phosphocreatine, 0.3 Na-GTP, 4 Mg-ATP, 10 HEPES. Osmolarity was adjusted to 280-290 mOsm and pH to 7.2-7.25. Electrical currents were acquired (Multiclamp 700B, Molecular Devices), sampled at 50 kHz, filtered at 4 kHz (voltage clamp) or 10 kHz (current clamp) (Digidata 1440 A, pClamp 10; Molecular Devices), and analyzed offline with Clampfit (Molecular Devices). Access resistance was monitored throughout experiments by injection of 5 mV hyperpolarizing current steps. When access resistance increased more than 20 % the protocol was terminated. To evoke action potentials in CCK_Ls 1200 pA currents steps of 2 ms duration were injected. For stimulating PNs, the pulse duration was increased to 4 ms. Connectivity was assessed by analysis of IPSCs in response to presynaptic bursts at 100 Hz for a duration of 50 ms every 10 s. At least 10 traces were recorded and averaged for each pair. For DSI protocols 20 Hz trains of 8 action potentials were elicited in CCK_Ls every 10 s. Due to variability in IPSC amplitude and occasional failures, the amplitude of postsynaptic responses to the presynaptic spike train was averaged in each trace. During

pharmacological experiments CCK_Ls were stimulated every 10 s with 2 action potentials of 45 ms inter-spike interval followed by a 500 ms break and 5 action potentials with 12.5 ms inter-spike interval. Spiking patterns were assessed by applying 40 current steps from -140 pA to 260 pA.

5. 2. 3. 4. Immunohistochemistry

Mice were anaesthetized with 3 % isoflurane followed by an injection of urethane (2.5 g/kg, i.p.). Animals were perfused with 4 % ice-cold paraformaldehyde in phosphate buffer (pH 7.4; 100 ml/animal) following an injection of 300 units heparin to the left ventricle. After 2 h postfixation, coronal brain sections (60 μm) were prepared with a vibratome (Leica Microsystems) and stored in PBS. Working solutions contained 0.5 % Triton in PBS and serum (where appropriate). Sections were incubated at 4 °C for 48 h with the following primary antibodies: chicken anti-GFP (1:1000; Invitrogen), rabbit anti-CCK (1:500; Frontiers Institute), guinea pig anti-PV (1:500; Synaptic Systems), rat anti-SOM (1:500; Millipore), mouse and rabbit anti-VGAT (1:300; Synaptic Systems), guinea pig anti-CB1R (1:500; Frontiers Institute), rabbit anti-DAGLα (1:500; Frontiers Institute), rabbit anti-MGL (1:500; Frontiers Institute). Subsequent secondary antibody incubation was carried out overnight at 4 °C with: goat anti-mouse 405 dylight (1:500; Thermo scientific), goat anti-rabbit Alexa 405, goat anti-rabbit Alexa 488, goat anti-chicken Alexa 488, goat anti-guinea pig Alexa 647, goat anti-rat Alexa 647, and goat anti-rat Alexa 568 (all 1:1000; Invitrogen). Sections were rinsed with PBS and mounted/coverslipped on glass slides. Confocal images were acquired using a LSM 700 microscope (Carl Zeiss) equipped with four laser lines (405, 488, 555, and 639 nm). For basic characterization of molecular marker expression in the BA of CCK-IN-GFP mice, sections were scanned with a 20x objective (Plan-Apochromat 20x/0.8 M27, Zeiss). Images of CB1R, DGlα, MGL and VGAT subcellular localization were acquired at 63x magnification (Plan-Apochromat 63x/1.40 Oil DIC objective, Zeiss), a pixel size of 80 nm, 1.3 optical zoom, pinhole 1 Airy unit and 200 nm z-sections. Images were deconvolved using Huygens Software (Scientific Volume imaging). Quantification was performed manually in a blind manner using

Imaris software (Bitplane AG). All focal planes of uncut cell bodies were analyzed. Statistical analysis was carried out with Graphpad Prism software.

5. 2. 4. Results

To probe the functional organization of CCK_L mediated inhibition onto defined populations of PNs, we performed paired whole-cell patch clamp recordings of CCK_Ls and retrogradely labeled projection neurons (*n* = 236) in acute brain slices of CCK-IN-GFP mice (Figure 13). Selective GFP expression in CCK INs was obtained via an intersectional approach, using CCK-IRES-Cre::Dlx-Flp::RCE:dual reporter mice (Miyoshi et al., 2010). GFP^+ neurons with somatic size similar to mPFC-projecting neurons (CCK_L 779.5 ± 18.9 μm^2, *n* = 119; $PN_{IL/PL}$ 777.7 ± 24.6 μm^2, *n* = 59) were considered as CCK_Ls (Figure 14) and targeted for subsequent experiments. Immunohistochemical analysis revealed a large overlap of GFP^+ INs with CCK, but not markers for other major subpopulations of amygdala INs expressing parvalbumin (PV) or somatostatin (SOM; Figure 14D, E). Consistent with CCK expression in some glutamatergic PNs (www.mouse.brain-map.org), around 30 % of CCK^+ cells were GFP^- (Figure 14D, E).

To record from identified PN_{PL}s and PN_{IL}s in *ex vivo* brain slices, fluorescent latex retrobeads were stereotaxically injected to IL or PL (Figure 15) two to seven days prior to recordings. Paired recordings from GFP^+ CCK_Ls and $bead^+$ PNs revealed robust, picrotoxin-sensitive GABAergic synaptic transmission from CCK_Ls to both IL- and PL-projecting PNs (Figure 13C, D) with a success rate of 96.28 % for $CCK_L \rightarrow PN_{IL}$ and 97.96 % for $CCK_L \rightarrow PN_{PL}$ synapses. Connection probability was similar for both PN populations ($CCK_L \rightarrow PN_{PL}$: 56.6 %, *n* = 145 tested pairs; $CCK_L \rightarrow PN_{IL}$: 58.5 %, *n* = 82, Figure 1E). Excitatory PN synapses onto CCK_Ls were observed less frequently, but with no significant difference between PN_{PL}s and PN_{IL}s ($PN_{PL} \rightarrow CCK_L$: 16.1 %, *n* = 112, $PN_{IL} \rightarrow CCK_L$: 22.2 %, *n* = 72 tested pairs). Synaptic conductance did not significantly differ between $CCK_L \rightarrow PN_{PL}$ and $CCK_L \rightarrow PN_{IL}$ pairs in response to single presynaptic action potentials (APs) or 50 ms, 100 Hz AP bursts (Figure 13F, G).

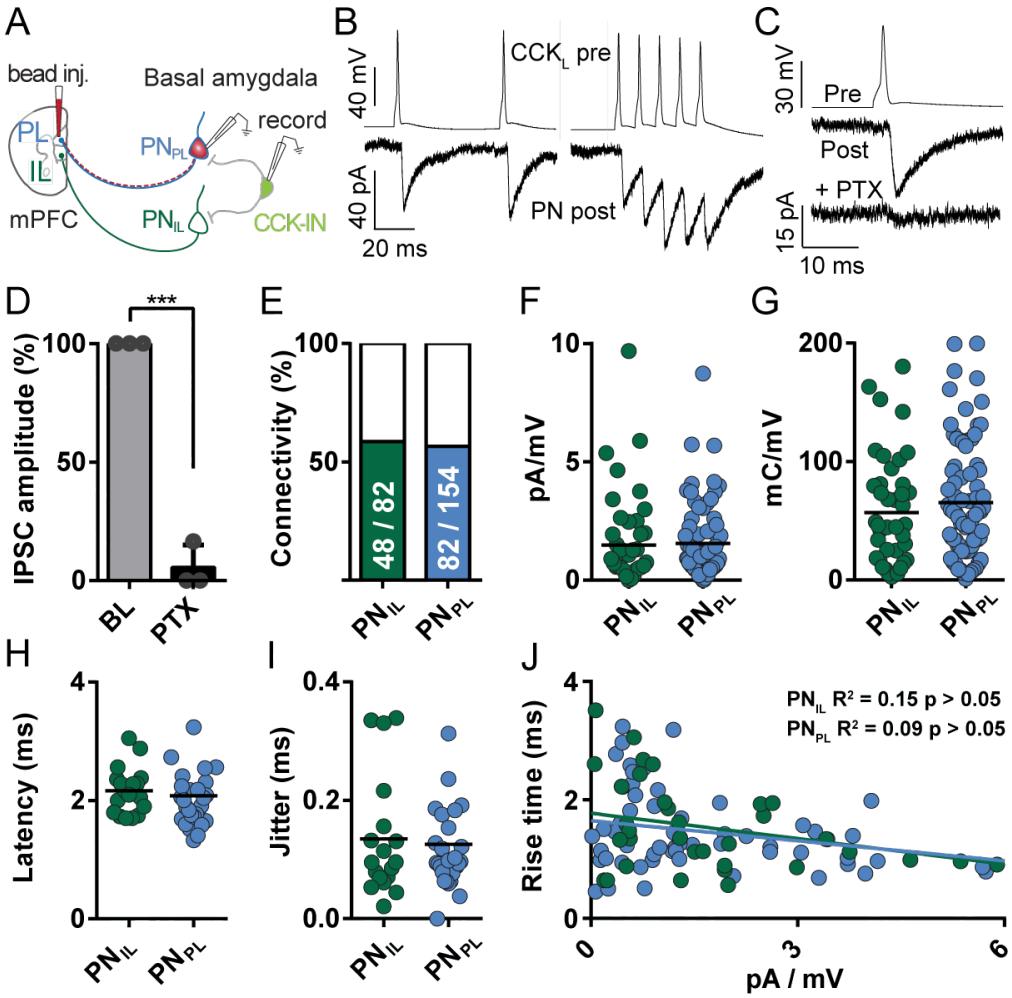

Figure 13. Uniform connectivity and strength of CCK_L synapses onto IL- and PL-projecting principal neurons in basal amygdala. (**A**) Experimental design. (**B**) Example traces; connectivity between GFP-positive CCK_Ls and retrobead-labeled PNs was assessed by eliciting two action potentials (APs) in the presynaptic cell (inter-spike-interval: 45 ms) followed by a burst of five APs (100 Hz, above). Resulting inhibitory postsynaptic currents were recorded in voltage clamp (below) (**C,D**) CCK_L→PN synaptic transmission is blocked by GABA-A receptor antagonist picrotoxin (PTX; 100 µM; n = 3, t-test $p < 0.0001$). (**E**) Connection probability for CCK_L→PN pairs is similar between PNs with different mPFC projection targets (CCK_L→PN_{PL}: 56.6%, n = 154 tested pairs; CCK_L→PN_{IL}: 58.5%, n = 82) (**F**) Synaptic conductance of CCK_L→PN unitary IPSCs. Slope was calculated from IPSC amplitude of three different holding levels (-50, -60, -70 mV; CCK_L→PN_{PL}: n = 69; CCK_L→PN_{IL}: n = 40; t-test $p > 0.05$) (**G**) Synaptic charge transfer resulting from a 100 Hz presynaptic burst. Slope was calculated from IPSC charge transfer (50 ms window after IPSC onset) at three different holding potentials (-50, -60, -70 mV; CCK_L→PN_{PL}: n = 82; CCK_L→PN_{IL}: n = 41; t-test $p > 0.05$). (**H**) IPSC latency did not differ between cell types (calculated from presynaptic AP threshold to IPSC onset (CCK_L→PN_{PL}: n = 28; CCK_L→PN_{IL}: n = 18; t-test $p > 0.05$). (**I**) Jitter was calculated as the standard deviation from IPSC latency and does not differ between groups (CCK_L→PN_{PL}: n = 28; CCK_L→PN_{IL}: n = 18; t-test $p > 0.05$). (**J**) Conductance of single IPSCs is not correlated with IPSC rise time (CCK_L→PN_{PL}: n = 58; R^2 = 0.15, $p > 0.05$; CCK_L→PN_{IL}: n = 36; R^2 = 0.09, $p > 0.05$); Data represent mean ± s.e.m., ***$p < 0.001$.

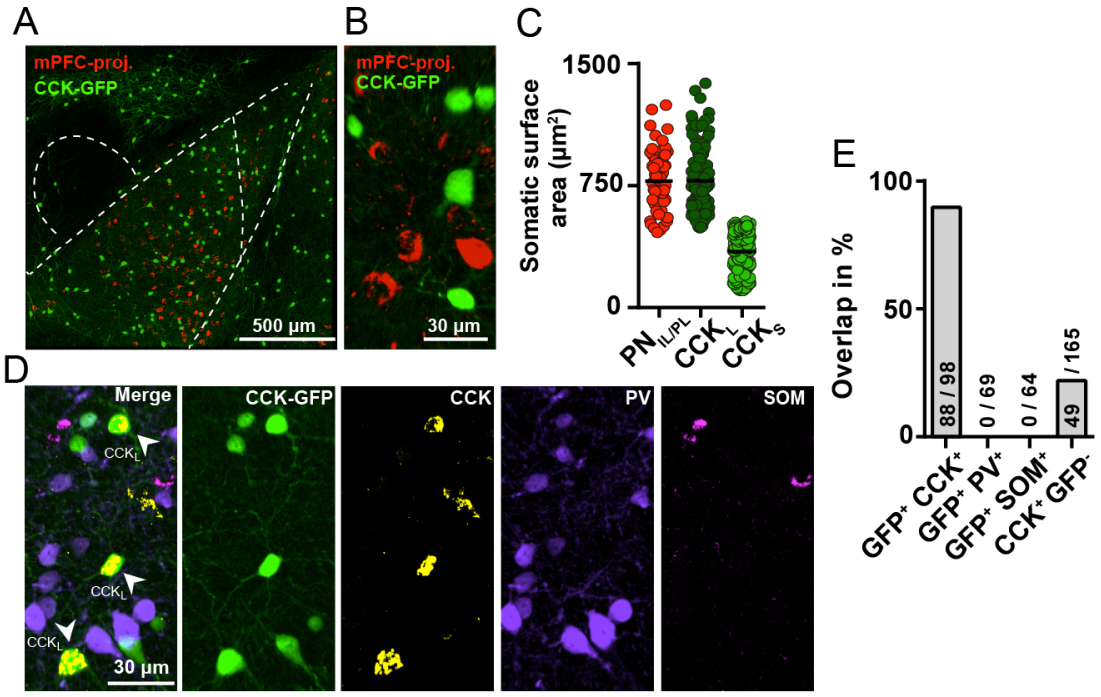

Figure 14. Selective Targeting of GFP expression to CCK-INs in the amygdala of *Dlx-Flp::CCK-IRES-Cre::RCE:dual* mice. (**A,B**) GFP$^+$ cells and CTX-B labelled mPFC-projecting neurons are intermingled in basal amygdala. (**C**) Graph shows the somatic surface area of mPFC-projecting PNs and visually identified large and small CCKs ($PN_{IL/PL}$, CCK_L, CCK_S). Data points represent individual cells ($PN_{IL/PL}$ n = 59, CCK_L n = 119, CCK_S n = 287) with bar overlay for group means. For all experiments GFP$^+$ neurons with a somatic size comparable to surrounding PNs were considered as CCK_Ls and targeted for recordings and analysis of molecular marker expression. (**D, E**) Quantification of immunoreactivity and GFP$^+$ labeling in BA reveals extensive somatic overlap of GFP with CCK but not SOM or PV.

Interestingly, unlike what has been observed for hippocampal CCK$^+$ INs (Hefft and Jonas, 2005), IPSC latency at CCK_L→$PN_{PL/IL}$ synapses was short (CCK_L→PN_{PL}: 2.08 ± 0.11 ms, n = 28; CCK_L→PN_{IL}: 2.16 ± 0.09 ms, n = 18; t-test $p > 0.05$) with low jitter (CCK_L→PN_{PL}: 0.13 ± 0.02 ms, n = 28; CCK_L→PN_{IL}: 0.14 ± 0.02 n = 18; t-test $p > 0.05$) but did not differ between groups (Figure 13H, I). No correlation between synaptic conductance and IPSC rise time, which would be a first indication for a heterogeneous distribution of synaptic location relative to the recording site, was observed. Also, values were similar for both postsynaptic PN populations (CCK_L→PN_{PL}: n = 58; R^2 = 0.15, $p > 0.05$; CCK_L→PN_{IL}: n = 36; R^2 = 0.09, $p > 0.05$; Figure 13J). Comprehensive analysis of cellular properties revealed significant differences between large and small CCKs but not between CCK_Ls targeting IL- or PL-projecting PNs (Table 1). Together, these results indicate that on the

level of unitary synaptic connectivity and strength, distinct subpopulations of mPFC-projecting BA principal neurons receive uniform, reliable, and rapid inhibition by CCK_Ls.

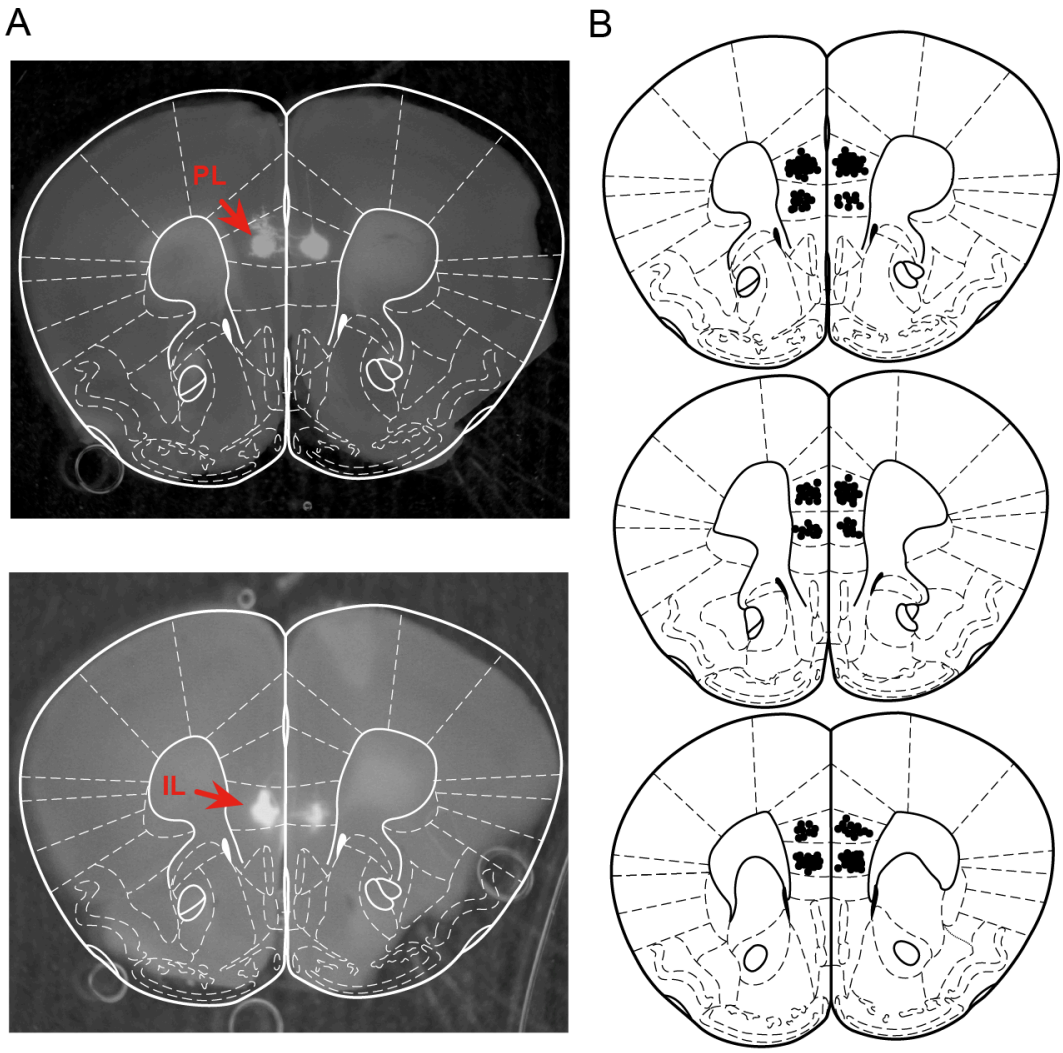

Figure 15. Retrobead injection sites in mPFC. (**A**) Examples of histological verification for IL and PL subdivision targeting. (**B**) Schematic representation of all injections used in experiments; dots indicate the center of the injection site. Atlas planes refer to 1.94 mm, 1.78 mm and 1.7 mm rostral from bregma (top to bottom).

Table 1. Basic properties of CCK_Ls targeting IL- or PL-projecting PNs and CCK_Ss. No significant difference was found between CCK_Ls targeting IL- or PL-projecting PNs. However, CCK_Ss exhibited significantly higher input resistance (R_{input}), broader action potentials (AP half-width), lower action potential amplitude, larger after-hyper-polarization (fAHP), larger sag and fired a higher number of action potentials (max. number of APs).

	CCK_L →PN_{IL}	**CCK_L →PN_{PL}**	**CCK_S**	**One-way ANOVA**	**Bonferroni post-hoc comparisons**
R_{input} MΩ	241.7 ± 13.1 *n* = 37	225.7 ± 9.5 *n* = 50	346.2 ± 26.3 *n* = 29	**$F_{2, 113}$ = 16.02 *p* < 0.0001**	$CCK_{L(IL)}$ vs. $CCK_{L(PL)}$ *p* > 0.05 **$CCK_{L(IL)}$ vs. CCK_S *p* < 0.0001** **$CCK_{L(PL)}$ vs. CCK_S *p* < 0.0001**
V_m (mV)	-64.6 ± 0.9 *n* = 37	-65.0 ± 1.0 *n* = 50	-63.2 ± 1.1 *n* = 29	$F_{2, 113}$ = 0.6512 *p* > 0.05	$CCK_{L(IL)}$ vs. $CCK_{L(PL)}$ *p* > 0.05 $CCK_{L(IL)}$ vs. CCK_S *p* > 0.05 $CCK_{L(PL)}$ vs. CCK_S *p* > 0.05
AP threshold (mV)	-40.0 ± 0.7 *n* = 37	-39.5 ± 0.6 *n* = 50	-38.4 ± 1.7 *n* = 29	$F_{2, 113}$ = 1.184 *p* > 0.05	$CCK_{L(IL)}$ vs. $CCK_{L(PL)}$ *p* > 0.05 $CCK_{L(IL)}$ vs. CCK_S *p* > 0.05 $CCK_{L(PL)}$ vs. CCK_S *p* > 0.05
AP half width (ms)	0.96 ± 0.04 *n* = 37	0.99 ± 0.03 *n* = 50	1.29 ± 0.06 *n*=29	**$F_{2, 113}$ = 14.58 *p* < 0.0001**	$CCK_{L(IL)}$ vs. $CCK_{L(PL)}$ *p* > 0.05 **$CCK_{L(IL)}$ vs. CCK_S *p* < 0.0001** **$CCK_{L(PL)}$ vs. CCK_S *p* < 0.0001**
AP amplitude (mV)	54.5 ± 1.6 *n* = 37	51.9 ± 1.6 *n* = 50	44.2 ± 2.0 *n* = 29	**$F_{2, 113}$ = 7.974 *p* < 0.001**	$CCK_{L(IL)}$ vs. $CCK_{L(PL)}$ *p* > 0.05 **$CCK_{L(IL)}$ vs. CCK_S *p* < 0.001** **$CCK_{L(PL)}$ vs. CCK_S *p* < 0.01**
fAHP (mV)	-17.1 ± 0.8 *n* = 37	-15.8 ± 0.5 *n* = 50	-13.1 ± 1.2 *n* = 29	**$F_{2, 113}$ = 5.774 *p* < 0.01**	$CCK_{L(IL)}$ vs. $CCK_{L(PL)}$ *p* > 0.05 **$CCK_{L(IL)}$ vs. CCK_S *p* < 0.01** $CCK_{L(PL)}$ vs. CCK_S *p* > 0.05
Max. number of APs	3.6 ± 0.5 *n* = 37	3.3 ± 0.4 *n* = 50	7.6 ± 1.4 *n* = 29	**$F_{2, 113}$ = 9.024 *p* < 0.001**	$CCK_{L(IL)}$ vs. $CCK_{L(PL)}$ *p* > 0.05 **$CCK_{L(IL)}$ vs. CCK_S *p* < 0.01** **$CCK_{L(PL)}$ vs. CCK_S *p* < 0.001**
Sag (mV)	2.6 ± 0.6 *n* = 37	1.6 ± 0.2 *n* = 50	3.9 ± 0.7 *n* = 29	**$F_{2, 113}$ = 5.019 *p* < 0.01**	$CCK_{L(IL)}$ vs. $CCK_{L(PL)}$ *p* > 0.05 $CCK_{L(IL)}$ vs. CCK_S *p* > 0.05 **$CCK_{L(PL)}$ vs. CCK_S *p* < 0.01**

Given the evidence for CB1R-dependent mechanisms in CKK IN mediated microcircuit regulation (Freund, 2003; Armstrong and Soltesz, 2012; Trouche et al., 2013) and amygdala-driven fear extinction processes (Marsicano et al., 2002), we assessed depolarization-induced suppression of inhibition (DSI), an endocannabinoid-dependent form of short-term plasticity (Ohno-Shosaku et al., 2001; Wilson and Nicoll, 2001; Wilson et al., 2001). To induce DSI, postsynaptic PNs were depolarized to 0 mV for 5 s to mimic strong postsynaptic activity (Figure 16A). At many CB1R-expressing interneuron synapses this acts as a trigger for postsynaptic endocannabinoid synthesis and release causing a transient CB1R-mediated suppression of presynaptic release probability (Wilson and Nicoll, 2002; Galarreta et al., 2008). In the BA, an immediate and robust decrease of IPSC amplitude following postsynaptic depolarization was recorded, which was completely prevented by application of CB1R antagonist AM251 (Figure 16C). While such DSI was observed at all $CCK_L \rightarrow PN_{IL}$ synapses $CCK_L \rightarrow PN_{PL}$ synapses were less frequently inhibited (Figure 16B). On average, DSI magnitude significantly differed between groups ($CCK_L \rightarrow PN_{IL}$: 92.6 ± 2.6 % DSI, $n = 20$; $CCK_L \rightarrow PN_{PL}$: 45.3 ± 10.9 %, $n = 33$; $p < 0.0001$, Two way ANOVA, Bonferroni post hoc comparison; Figure 16D). Consistent with the differential sensitivity to DSI, $CCK_L \rightarrow PN_{IL}$ synapses exhibited stronger depression upon presynaptic high-frequency bursts (Figure 17). Thus, in contrast to the uniform synaptic connectivity and strength, dynamic regulation of CCK_L synapses depends on the identity of the postsynaptic target cell with $CCK_L \rightarrow PN_{IL}$ synapses being more susceptible to activity-dependent suppression.

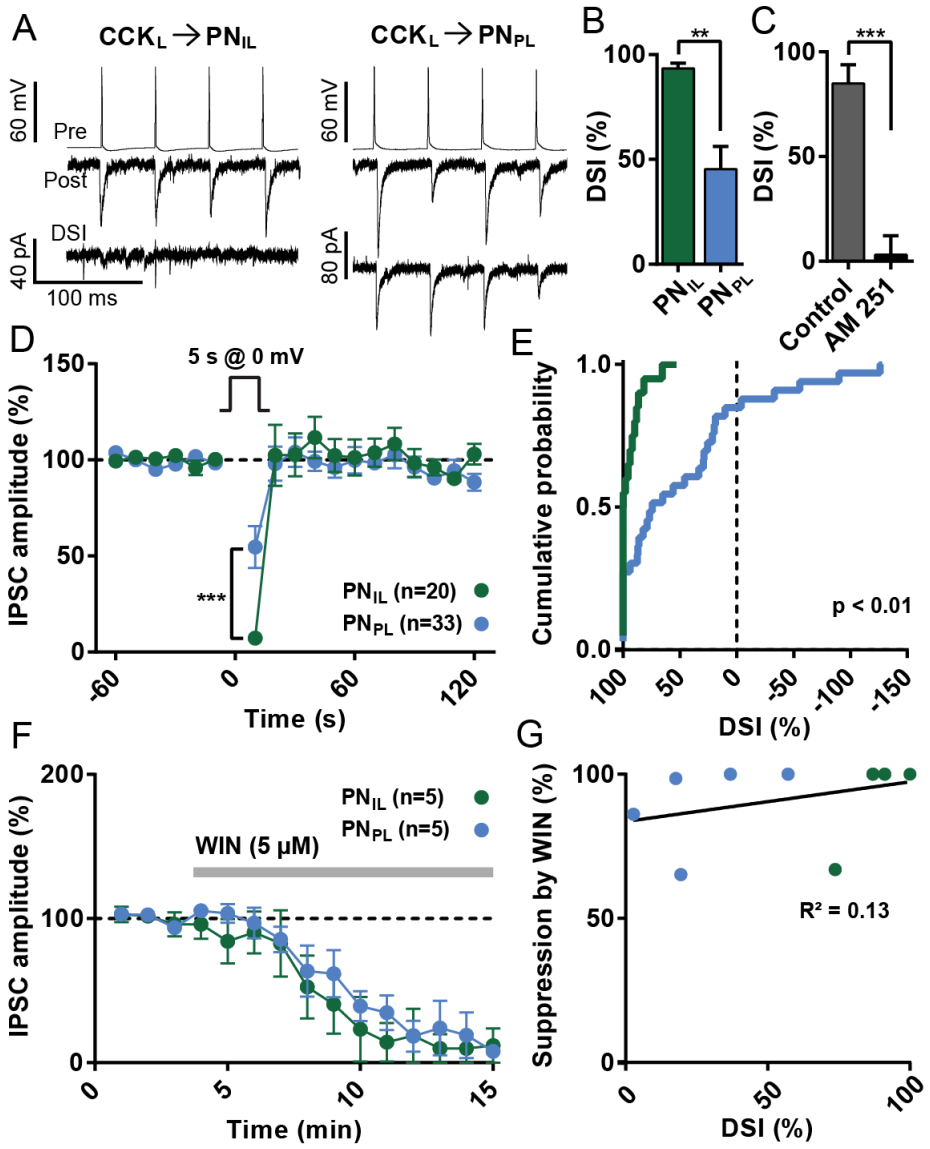

Figure 16. Projection target-dependent asymmetric expression of retrograde endocannabinoid signaling at CCK$_L$→PN synapses. (**A**) Example traces showing depolarization-induced suppression of inhibition (DSI) at CCK$_L$→PN$_{IL}$ and CCK$_L$→PN$_{PL}$ synapses. IPSCs were evoked by trains of eight APs at 20 Hz in presynaptic CCK$_L$s every 10 s. To induce DSI PNs were depolarized to 0 mV for 5 s. Postsynaptic IPSC amplitudes during each train are averaged to form each data point. (**B**) Circuit-specific differences in DSI expression. DSI is expressed as percent decrease in mean IPSC amplitude of the first train following PN depolarization compared with preceding 60 s baseline recording (CCK$_L$→PN$_{IL}$: n = 20; CCK$_L$→PN$_{PL}$: n = 33; t-test $p < 0.01$) (**C**) DSI at CCK$_L$→PN synapses is abolished by perfusion of CB1R antagonist AM251 (10 µM; n = 3, t-test $p < 0.001$ (**D**) Time course of IPSC suppression following DSI induction at CCK$_L$→PN synapses (CCK$_L$→PN$_{IL}$: n = 20; CCK$_L$→PN$_{PL}$: n = 33; Two-way ANOVA $F_{1,51} = 0.005$, $p > 0.05$, post hoc Bonferroni multiple comparisons $p < 0.0001$). (**E**) Distribution of DSI magnitudes for PN projection classes (CCK$_L$→PN$_{IL}$: n = 20; CCK$_L$→PN$_{PL}$: n = 33; Kolmogorov-Smirnov $p < 0.01$). (**F**) Suppression of synaptic transmission by application of CB1R agonist WIN55,212-2 (WIN; 5 µM; CCK$_L$→PN$_{IL}$: n = 5; CCK$_L$→PN$_{PL}$: n = 5; Two-way ANOVA $F_{1,8} = 0.7201$, $p > 0.05$). (**G**) No significant correlation between DSI magnitude and WIN-induced reduction in IPSC amplitude (linear regression, p > 0.05). Grouped data represented as mean ± s.e.m., $^{**}p < 0.01$, $^{***}p < 0.001$.

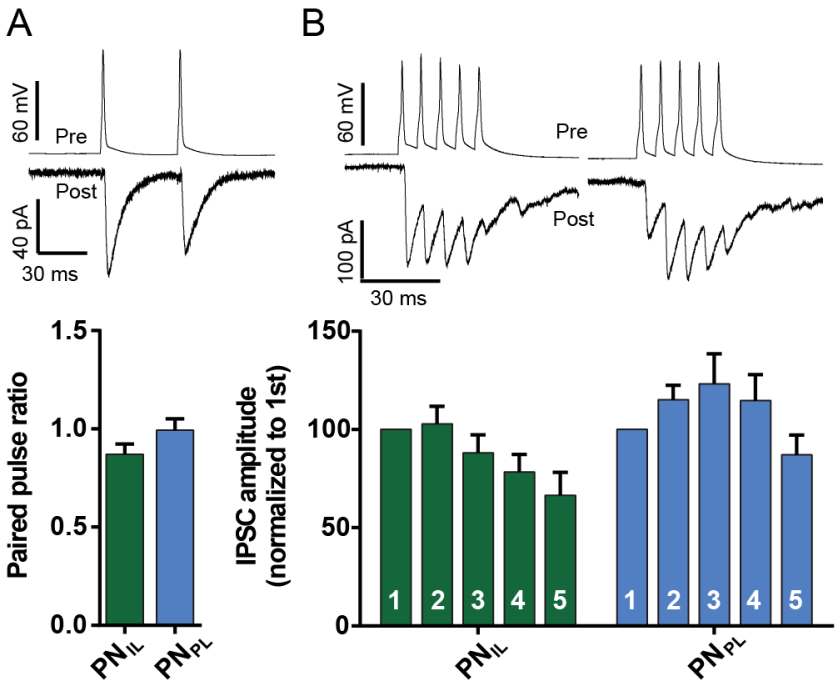

Figure 17. Short-term plasticity of CCK_L-IN→$PN_{PL/IL}$ synapses. (**A**) Example traces (above) and quantification (below) of paired pulse ratio; CCK_Ls were driven to fire action potentials (AP) with an inter spike interval of 45 ms. Paired-pulse ratio (2nd IPSC amplitude over 1st IPSC amplitude) for cells recorded from each postsynaptic target group did not significantly differ (CCK_L→PN_{IL}: n = 43; CCK_L→PN_{PL}: n = 67; t-test $p > 0.05$ (**B**) CCK_L→$PN_{PL/IL}$ IPSC dynamics in response to 100 Hz AP bursts; Amplitude of the 1st IPSC was measured from baseline, IPSCs 2-5 were measured from peak of decay of preceding IPSC to maximum amplitude and normalized to IPSC 1. CCK_L→PN_{IL} synapses exhibit IPSC amplitude depression compared with CCK_L→PN_{PL} synapses. (CCK_L→PN_{IL}: n = 35; CCK_L→PN_{PL}: n = 59; two-way ANOVA $_{F1, 460}$ = 9.284, $p < 0.01$). Data represented as mean + s.e.m..

These results raise the question whether pre- or postsynaptic factors underlie the target-specificity of DSI. To explore whether differential CB1R expression or tonic CB1R activation could account for alterations in DSI, CB1R agonist WIN55,212-2 (5 µM) was applied during paired recordings. We observed that CCK_L-IPSCs onto PN_{PL} and PN_{IL}s were depressed with similar effect magnitude and time course (Figure 16F). No correlation of suppression by WIN and DSI magnitude was observed (Figure 16G). Additionally, we tested whether CCK_L synapses are tonically suppressed by endocannabinoids. However, application of AM251 (10 µM) had no effect on IPSC amplitude for either postsynaptic target (CCK_L→PN_{IL} 12.2 ± 19.6 %, n = 5; CCK_L→PN_{PL} 0.5 ± 22.1 %, n = 4) Together, these results suggest that lower DSI levels in PL-projecting cells is not explained by a presynaptic mechanism.

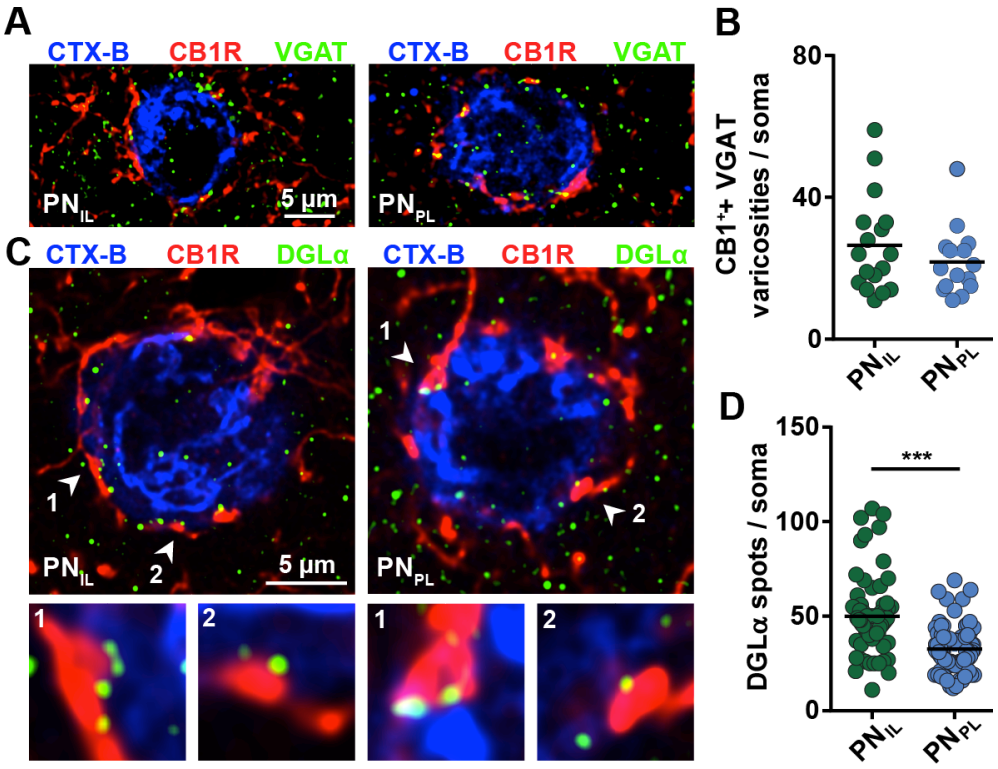

Figure 18. Projection-specific expression of endocannabinoid synthesizing enzyme DGLα. Projection-specific expression of endocannabinoid synthesizing enzyme DGLα. (**A**) Example images of CB1R and VGAT immunohistochemical detection in BA sections containing retrogradely labeled IL- and PL-projecting PNs; a single focal plane (200 nm) is shown. Blue: CTX-B, red: CB1R, green: VGAT. (**B**) Number of bouton-like appositions co-expressing CB1R and VGAT does not differ at PN_{IL} and PN_{PL} somata (PN_{IL}: n = 33; PN_{PL}: n = 29; t-test $p > 0.05$) (**C**) Example images illustrating DGLα expression in IL- and PL-projecting PNs; smaller panels depict higher magnification images of somatic appositions indicated with arrows; single focal planes (200 nm) are shown. (**D**) A significantly greater number of DGLα^{+} puncta in apposition to CB1R^{+} varicosities are detected in PN_{IL}s (PN_{IL}: n = 64; PN_{PL}: n = 88; t-test $p < 0.0001$). Data points represent counts obtained from individual cells with bar overlay for group means, ***$p < 0.001$.

To address whether postsynaptic differences in IL- vs. PL-projecting PNs could account for altered endocannabinoid signaling, we examined the subcellular expression of synthesis (diacylglycerol lipase α; DGLα) and degradation (monoacylglycerol lipase; MGL) enzymes for 2-arachidonylglycerol, the main endocannabinoid contributing to DSI at central synapses (Hashimotodani et al., 2008; Tanimura et al., 2010). Using immunohistochemistry, we first quantified co-expression of the vesicular GABA transporter (VGAT) in CB1R^{+} bouton-like appositions on the somatic surface of Choleratoxin-B labeled IL- and PL-projecting PNs (Figure 18A, B).

98.2 ± 0.5 % of CB1R$^+$ varicosities were also immunoreactive for VGAT indicating that the vast majority of somatic CB1R$^+$ contacts reflect synapses from GABAergic neurons. No difference in the number of CB1R$^+$ bouton-like appositions could be detected between IL- and PL-projecting PNs (PN_{IL}: 28.5 ± 2.2, n = 33; PN_{PL}: 24.2 ± 1.7, n = 29; t-test $p > 0.05$) Next, we quantified DGLα^+ puncta closely apposed to CB1R$^+$ boutons at the cell surface of postsynaptic IL- or PL-projecting PNs. Blinded analysis revealed 43.9 ± 2.3 % lower DGLα expression in PL-projecting cells (Figure 18C, D). Similar results were obtained in triple-labeled sections in which somatic DGLα^+ appositions to double-labeled VGAT$^+$/CB1R$^+$ boutons were quantified (Figure 19). No difference in presynaptic MGL expression was observed (Figure 20).

Together, these findings indicate that postsynaptic expression of 2-arachidonylglycerol synthesis enzyme DGLα is determined by neuronal projection target in the BA, and that functional specificity of projection pathways is, at least in part, determined by postsynaptic differences in signaling.

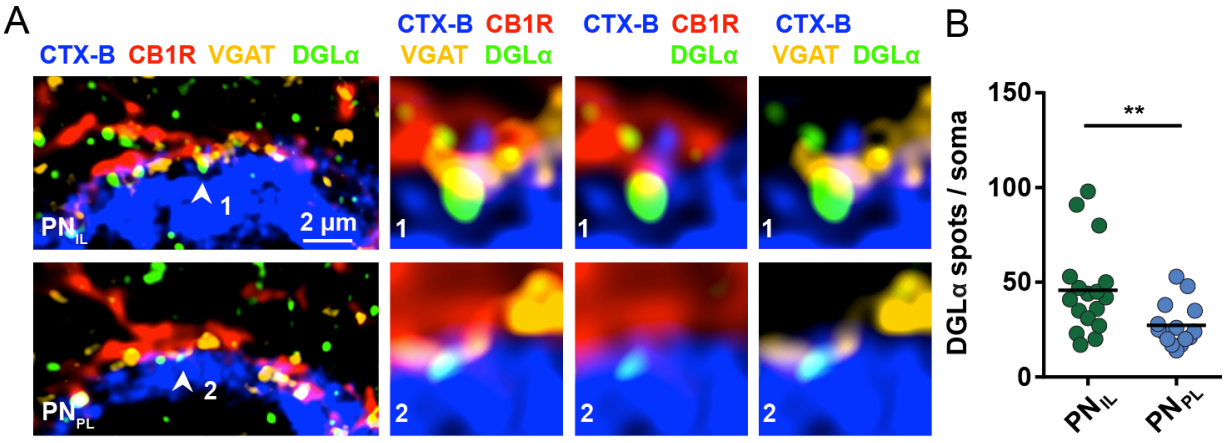

Figure 19. Quadruple-label immunohistochemical analysis of CB1R, VGAT and DGLα in IL- and PL-projecting neurons. (**A**) Example images of DGLα, CB1R, and VGAT immunohistochemical detection in BA sections containing retrogradely labeled IL- or PL-projecting PNs; single (200 nm) focal plane (blue, CTX-B; red, CB1R; yellow, VGAT; green, DGLα). (**B**) Enrichment of somatic DGLα^+ appositions to double-labeled VGAT$^+$/CB1R$^+$ boutons in PN_{IL}s (PN_{IL}: n = 17; PN_{PL}: n = 15; t-test $p < 0.01$). Data points represent puncta counts obtained from individual cells with bar overlay for group means, $^{**}p < 0.01$.

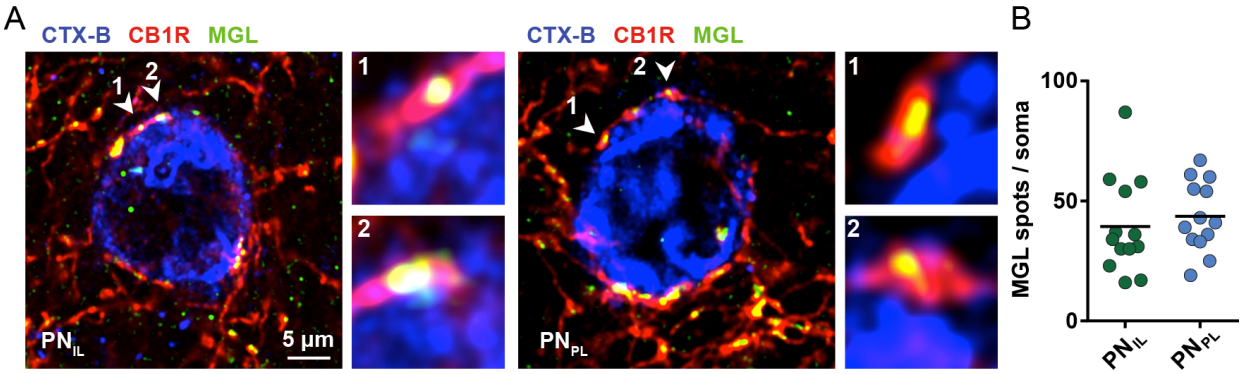

Figure 20. Similar expression of presynaptic MGL in bouton-like structures surrounding IL- and PL-projecting PNs. (**A**) Example images of MGL and CB1R immunohistochemical detection in BA sections containing retrogradely labeled IL- or PL-projecting PNs; single (200 nm) focal plane (blue, CTX-B; red, CB1R; green/yellow, MGL). (**B**) Quantification data indicating similar abundance of MGL in CB1R containing terminals onto both mPFC-projecting PN types (PN_{IL}: n = 13; PN_{PL}: n = 13; t-test $p > 0.05$). Data points represent puncta counts obtained from individual cells with bar overlay for group means.

5. 2. 5. Discussion

CCK_Ls have been proposed to be major regulators of fear extinction circuits (Marsicano et al., 2002) and emotional states (Freund, 2003). However, until recently, investigating their functional role was impeded by a lack of specific genetic tools. Using an intersectional genetic strategy, we were able to achieve targeted patch-clamp recordings of CCK_Ls and IL-/PL-projecting PNs to study the cell type-specific organization of CCK_L-mediated inhibitory synaptic transmission in fear extinction micro-circuits of the mouse amygdala.

We observed that CCK_Ls uniformly inhibit mPFC-projecting PNs with similar connectivity and synaptic strength. Furthermore, we did not discover any differences in CCK_L spiking properties targeting either postsynaptic cell type. This data suggest that CCK_Ls targeting mPFC-projecting PNs are a rather homogeneous population of interneurons and asymmetries promoting fine-tuning of output pathways might not be present on the level of absolute connectivity. Yet, based on our data we cannot exclude that amygdala CCK_Ls, similar to $CB1R^+$/$VGlut3^+$ CCK interneurons in entorhinal cortex (Varga et al., 2010), could exhibit target-specificity with regard to PNs projecting to brain regions other than mPFC.

Further, as recently reported for hippocampal CCK INs (Dudok et al., 2014), it is possible, that amygdala CCK_Ls are heterogeneous with distinct subtypes inhibiting different neuronal sub-compartments. Therefore, we analyzed whether rise time correlates with IPSC conductance, which would be a first indication that IPSCs originate at different relative electrotonic distances from the recording site. However, no such correlation was found, also values are similar for PN_{PL}s and PN_{IL}s and neither rise time nor IPSC amplitude correlate with expression of DSI, indicating that the asymmetry in DSI is unlikely to be explained by differences in CCK_L subtypes.

In contrast to the unitary connectivity and synaptic strength, we found that the dynamics of CCK_L-mediated synaptic inhibition onto distinct subpopulations of BA projection neurons are cell type- and pathway-specific. Both short-term synaptic plasticity and DSI are different for BA neurons projecting to either PL or IL. $CCK_L \rightarrow PN_{IL}$ synapses exhibit depressing short-term plasticity dynamics in response to presynaptic high frequency spike trains as well as consistent and robust activity-dependent retrograde signaling. In contrast, $CCK_L \rightarrow PN_{PL}$ synapses show facilitating compound IPSCs and a significantly weaker DSI.

In terms of the underlying mechanism, and in line with the notion that PN_{PL}s and PN_{IL}s are contacted by a similar population of CCK_Ls, we found that $CCK_L \rightarrow PN_{PL}$ synapses and $CCK_L \rightarrow PN_{IL}$ synapses are equally suppressed in response to the application of an exogenous CB1R antagonist, and that the expression of the presynaptic endocannabinoid-degrading enzyme MGL is similar at $CCK_L \rightarrow PN_{PL}$ and $CCK_L \rightarrow PN_{IL}$ synapses. In contrast, the postsynaptic expression of the endocannabinoid-synthesizing enzyme DGLα is significantly greater in PN_{IL}s compared to PN_{PL}s, suggesting that cell type-specific differences in the postsynaptic endocannabinoid signaling machinery is an important factor determining the specificity of CB1R-mediated signaling in amygdalar circuits.

As previously described, the balance of activity between IL- and PL-projecting BA PNs is an important regulator determining the efficiency and strength of fear extinction learning (Senn et al., 2014). In the light of our present results, it is possible that during extinction learning, when IL-

projecting BA neurons are strongly activated (Senn et al., 2014), input from CCK_Ls onto IL-projecting PNs could rapidly be suppressed by activity-dependent mechanisms including short-term depression and DSI.

This cell-type specific short-term synaptic plasticity may function as a general mechanism to transform uniform recruitment of CCK_Ls into asymmetric inhibitory input onto projection-specific subpopulations of principal neurons. This projection-specific shift in the balance between inhibition and disinhibition via DSI could enhance contrast in activity between distinct output pathways to promote rapid behavioral adaptations.

5. 2. 6. Author contributions

E.V., S.K., J.G. and A.L. designed the experiments. E.V. performed the experiments and analyzed the data. E.V., J.I.W.C. and A.L. wrote the paper.

5. 2. 7. Acknowledgements

We would like to thank T. Klausberger and all members of the Lüthi lab for discussions and critical comments on the manuscript, the FMI microscopy facility for support with image acquisition and analysis, and J. Huang, G. Fishell and S. Arber for providing mouse lines. This work was supported by the Novartis Research Foundation, by the National Center of Competences in Research: ‘SYNAPSY - The Synaptic Bases of Mental Diseases’ (financed by the Swiss National Science Foundation), by an SNSF core grant (to A.L.), and by fellowships from EMBO (to J.G.), Marie Curie Actions (to J.G.) and the Canadian Institutes for Health Research (to J.I.W.C.).

5. 2. 8. Additional results

5. 2. 8. 1. Characterization of basal amygdala CCK_Ls

Paired recordings of basal amygdala CCK_Ls revealed both chemical and electrical synapses between interneurons (Fig. 21A, B). Gap junctions were observed in 28.6 % of tested pairs. Connection probability of GABAergic synapses between CCK_Ls was higher than for mPFC projecting PNs as postsynaptic targets ($CCK_L \rightarrow CCK_L$ 82.35 %, n = 51 tested pairs; $CCK_L \rightarrow PN_{PL}$: 56.6 %, n = 145; $CCK_L \rightarrow PN_{IL}$: 58.5 %, n = 82).

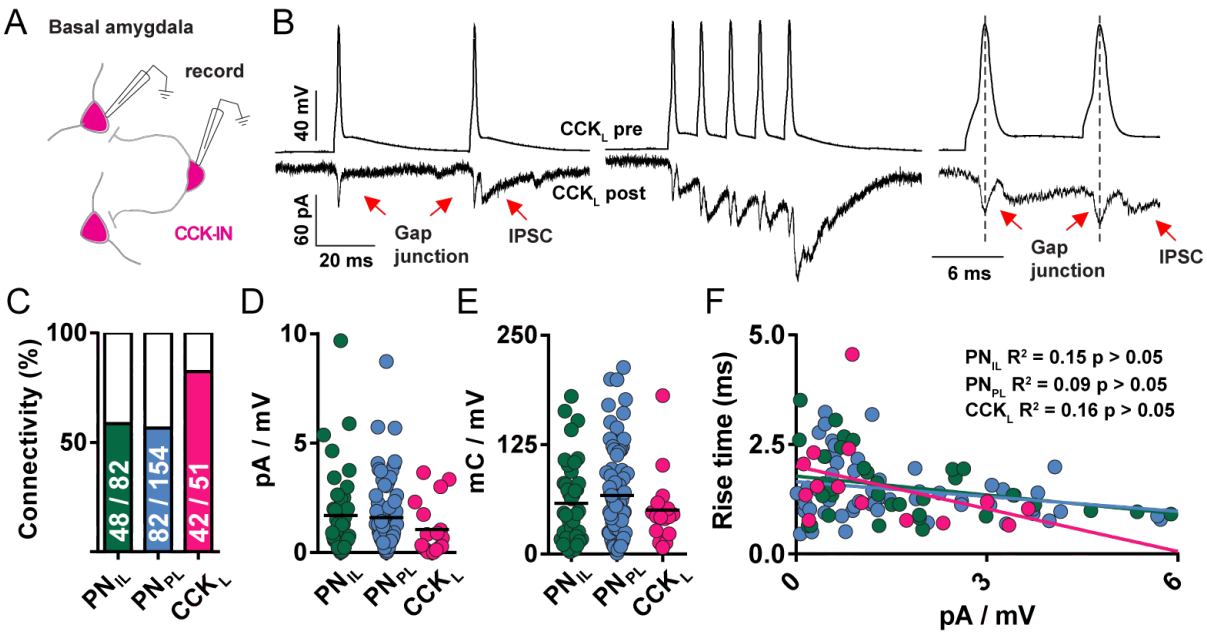

Figure 21. CCK_Ls in basal amygdala are highly interconnected with chemical and electrical synapses. Data for mPFC-projecting PNs as shown before; (**A**) Experimental design. (**B**) Example traces; connectivity between GFP-positive CCK_Ls was assessed by eliciting two action potentials (APs) in the presynaptic cell (inter-spike-interval: 45 ms) followed by a burst of five APs (100 Hz, above). Resulting inhibitory postsynaptic currents were recorded in voltage clamp (below). Red arrows indicate gap junctions followed by IPSCs. (**C**) Connection probability for $CCK_L \rightarrow CCK_L$ pairs is higher than for $CCK_L \rightarrow$PN pairs ($CCK_L \rightarrow CCK_L$ 82.35 %, n = 51; $CCK_L \rightarrow PN_{PL}$: 56.6 %, n = 154 tested pairs; $CCK_L \rightarrow PN_{IL}$: 58.5 %, n = 82) (**D**) Synaptic conductance of unitary IPSCs. Slope was calculated from IPSC amplitude of three different holding levels (-50, -60, -70 mV; $CCK_L \rightarrow CCK_L$: n = 18; $CCK_L \rightarrow PN_{PL}$: n = 69; $CCK_L \rightarrow PN_{IL}$: n = 40; One-way ANOVA $F_{2,124}$ = 0.976, p > 0.05) (**E**) Synaptic charge transfer resulting from a 100 Hz presynaptic burst. Slope was calculated from IPSC charge transfer (50 ms window after IPSC onset) at three different holding potentials (-50, -60, -70 mV; $CCK_L \rightarrow CCK_L$: n = 16; $CCK_L \rightarrow PN_{PL}$: n = 82; $CCK_L \rightarrow PN_{IL}$: n = 41; One-way ANOVA $F_{2,135}$ = 0.999, p > 0.05). (**F**) Conductance of single IPSCs is not correlated with IPSC rise time ($CCK_L \rightarrow CCK_L$ n = 14; R_2 = 0.15, p > 0.05; $CCK_L \rightarrow PN_{PL}$: n = 58; R^2 = 0.15, p > 0.05; $CCK_L \rightarrow PN_{IL}$: n = 36; R^2 = 0.09, p > 0.05); Data represent mean ± s.e.m..

Conductance of IPSCs evoked by single IPSCs and 100 Hz spike trains did not differ from synaptic strength of $CCK_L \rightarrow PN_{PL/IL}$ synapses (single IPSC $CCK_L \rightarrow CCK_L$ 1.09 ± 0.29 pA/mV, *n* = 18; $CCK_L \rightarrow PN_{PL}$ 1.60 ± 0.20 pA/mV, *n* = 69; $CCK_L \rightarrow PN_{IL}$ 1.70 ± 0.31 pA/mV, *n* = 40; 100 Hz burst $CCK_L \rightarrow CCK_L$ 50.21 ± 10.46 mC/mV, *n* = 16; $CCK_L \rightarrow PN_{PL}$ 66.92 ± 5.78 mC/mV, *n* = 81; $CCK_L \rightarrow PN_{IL}$ 57.91 ± 7.26 mC/mV, *n* = 41; Fig. 21D, E). Similar to $CCK_L \rightarrow PN_{PL/IL}$ pairs, no correlation of synaptic conductance and IPSC rise time was detected and $CCK_L \rightarrow CCK_L$ p synapses (Fig. 21F).

Compared with $CCK_L \rightarrow PN_{PL/IL}$ pairs $CCK_L \rightarrow CCK_L$ synapses showed the weakest suppression of inhibition in response to postsynaptic depolarization ($CCK_L \rightarrow CCK_L$: 24.3 ± 6.6 % DSI, *n* = 7; $CCK_L \rightarrow PN_{IL}$: 92.6 ± 2.6 % DSI, *n* = 20; $CCK_L \rightarrow PN_{PL}$: 45.3 ± 10.9 %, *n* = 33; Fig 22). This is consistent with previous studies reporting that DGLα is not expressed in amygdala interneurons (Yoshida et al. 2011). However, application of WIN completely blocked GABAergic transmission at interneuron-interneuron synapses, which is not correlated with DSI. Together this data suggest that CCK_Ls express presynaptic CB1Rs independent of the postsynaptic target.

As described before, $CCK_L \rightarrow PN_{IL}$ synapses exhibited the strongest reduction in inhibition to DSI and consistently expressed robust IPSC depression following 100 Hz spike trains (Fig 23B). Whereas $CCK_L \rightarrow PN_{PL}$ pairs show only moderate DSI and facilitating-depressing compound IPSCs, DSI at $CCK_L \rightarrow CCK_L$ synapses elicits the weakest suppression of inhibition but 100 Hz AP bursts evoke strongly facilitating synapses (Fig 23B). These findings further support the idea that uniform synaptic strength is contrasting the dynamic regulation of CCK_L synapses, which depends on the identity of the postsynaptic target.

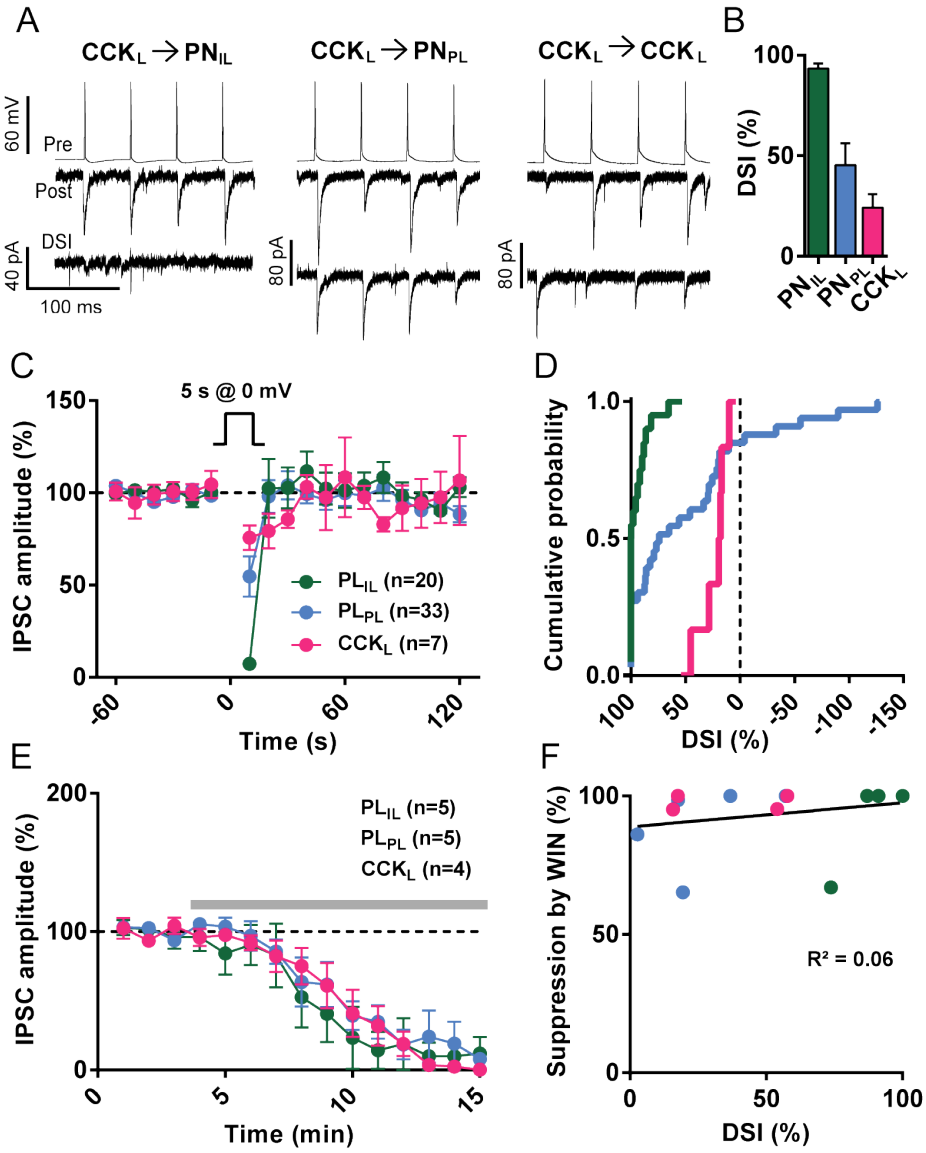

Figure 22. Asymmetric expression of retrograde endocannabinoid signaling at CCK$_L$→CCK$_L$ versus CCK$_L$→PN synapses. Data from CCK$_L$→PN pairs as shown before (**A**) Example traces showing depolarization-induced suppression of inhibition (DSI) at CCK$_L$→PN$_{IL}$ and CCK$_L$→PN$_{PL}$ and CCK$_L$→CCK$_L$ synapses. IPSCs were evoked by trains of eight APs at 20 Hz in presynaptic CCK$_L$s every 10 s. To induce DSI PNs were depolarized to 0 mV for 5 s. Postsynaptic IPSC amplitudes during each train are averaged to form each data point. (**B**) Circuit-specific differences in DSI expression. DSI is expressed as percent decrease in mean IPSC amplitude of the first train following PN depolarization compared with preceding 60 s baseline recording (CCK$_L$→CCK$_L$: 24.3 ± 6.6 % DSI, n = 7; CCK$_L$→PN$_{IL}$: n = 20; CCK$_L$→PN$_{PL}$: n = 33; One-way ANOVA $F_{2, 57}$ = 8.372, Bonferroni post hoc comparison PN$_{PL}$ vs. CCK$_L$ p > 0.05, PN$_{PL}$ vs. PN$_{IL}$ p < 0.01, PN$_{IL}$ vs. CCK$_L$ p < 0.01) (**C**) Time course of IPSC suppression following DSI induction at CCK$_L$→PN synapses (CCK$_L$→CCK$_L$: n = 7; CCK$_L$→PN$_{IL}$: n = 20; CCK$_L$→PN$_{PL}$: n = 33; Two-way ANOVA $F_{2, 57}$ = 0.01452, p > 0.05, post hoc Bonferroni multiple comparisons PN$_{PL}$ vs. CCK$_L$ p > 0.05, PN$_{PL}$ vs. PN$_{IL}$ p < 0.0001, PN$_{IL}$ vs. CCK$_L$ p < 0.0001). (**D**) Distribution of DSI magnitudes for all groups (CCK$_L$→CCK$_L$: n = 7; CCK$_L$→PN$_{IL}$: n = 20; CCK$_L$→PN$_{PL}$: n = 33). (**E**) Suppression of synaptic transmission by application of CB1R agonist WIN55,212-2 (WIN; 5 μM; CCK$_L$→CCK$_L$: n = 4; CCK$_L$→PN$_{IL}$: n = 5; CCK$_L$→PN$_{PL}$: n = 5; Two-way ANOVA $F_{2, 11}$ = 0.4288 p > 0.05). (**F**) No significant correlation between DSI magnitude and WIN-induced reduction in IPSC amplitude (linear regression p > 0.05). Grouped data represented as mean ± s.e.m., ***p < 0.0001.

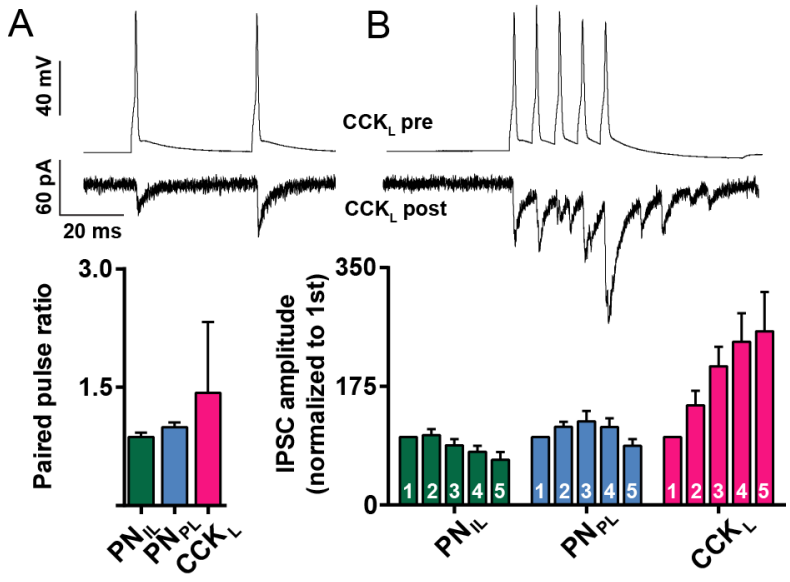

Figure 23. Short-term plasticity of CCK$_L$ synapses. Data from CCK$_L$→PN pairs as shown before (**A**) Example traces (above) and quantification (below) of paired pulse ratio; CCK$_L$s were driven to fire action potentials (AP) with an inter spike interval of 45 ms. Paired-pulse ratio (2nd IPSC amplitude over 1st IPSC amplitude) for PN$_{PL/IL}$s significantly differed from CCK$_L$s (CCK$_L$→CCK$_L$: n = 23; CCK$_L$→PN$_{IL}$: n = 43; CCK$_L$→PN$_{PL}$: n = 67; One-way ANOVA $F_{2, 130}$ = 8.175, p < 0.001, post hoc Bonferroni multiple comparisons PN$_{PL}$ vs. CCK$_L$ p < 0.01, PN$_{PL}$ vs. PN$_{IL}$ p > 0.05, PN$_{IL}$ vs. CCK$_L$ p < 0.001 (**B**) IPSC dynamics in response to 100 Hz AP bursts; Amplitude of the 1st IPSC was measured from baseline, IPSCs 2-5 were measured from peak of decay of preceding IPSC to maximum amplitude and normalized to IPSC 1. CCK$_L$→CCK$_L$ pairs show facilitating synapses in comparison to CCK$_L$→PN$_{IL}$ and CCK$_L$→PN$_{PL}$ synapses (CCK$_L$→CCK$_L$: n = 25; CCK$_L$→PN$_{IL}$: n = 35; CCK$_L$→PN$_{PL}$: n = 59; Two-way ANOVA $F_{2, 116}$ = 14.15, p < 0.0001). Data represented as mean ± s.e.m.

5. 2. 8. 2. Expression of DSI in IL- and PL-projecting PNs with extracellular stimulation

In a different set of experiments single PN$_{IL}$s and PN$_{PL}$s were recorded in basal amygdala. A bipolar stimulation electrode was placed in the vicinity of the recorded neuron to stimulate a variety of local inhibitory interneurons. Excitatory transmission was blocked by application of CPP (20 µM) and CNQX (20 µM). The DSI protocol revealed similar projection specific differences as observed in paired recordings. Depolarization of PN$_{PL}$s did not result in suppression of inhibition, whereas evoked IPSCs were decreased by activation on PN$_{IL}$s (PN$_{IL}$: 22.6 ± 7.1 % DSI, n = 11; PN$_{PL}$: -10.1 ± 9.5 % n = 11; t-test p < 0.05; Fig 24C).

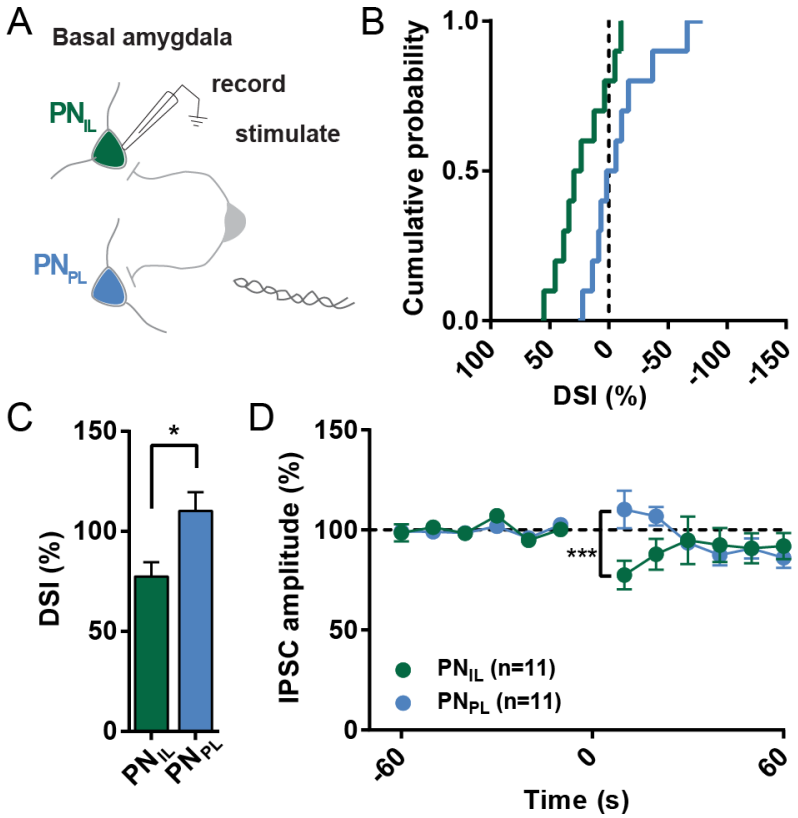

Figure 24. Projection target-dependent asymmetric expression of retrograde endocannabinoid signaling with extracellular stimulation of local GABAergic neurons. (**A**) Experimental design. IPSCs were evoked with a bipolar stimulation electrode in the vicinity of the recorded neuron. A small current was applied every 10 s to evoke a single IPSC. Baseline was recorded for 60 seconds. To induce DSI PNs were depolarized to 0 mV for 5 s. (**B**) Distribution of DSI magnitudes (PN_{IL} n = 11; PN_{PL}: n = 11; Kolmogorov-Smirnov p > 0.05). (**C**) Projection-specific differences in DSI expression. DSI is expressed as percent decrease in IPSC amplitude following depolarization compared with preceding 60 s baseline recording (PN_{IL}: 22.6 ± 7.1 % DSI, n = 11; PN_{PL}: -10.1 ± 9.5 % n = 11; t-test p < 0.05) (**D**) Time course of IPSC suppression following DSI induction (PN_{IL} n = 11; PN_{PL}: n = 11; Two-way ANOVA $F_{1, 20}$ = 1.059, post hoc Bonferroni multiple comparisons p < 0.001). Data represented as mean ± s.e.m. *p < 0.05, ***p < 0.001

5. 2. 8. 3. Effect of CCK on pyramidal neurons

In the amygdala CB1Rs are highly colocalized with CCK an anxiogenic neuropeptide (Mascagni & McDonald, 2003). The release mechanism is activity dependent, yet not fully understood. CCK has anxiogenic effects and opposite impact on fear extinction behavior compared to endocannabinoids. Intracerebroventricular injections of CCK agonist pentagastrin dose-dependently impaired extinction learning. On the other hand, systemic

injection of CB1 antagonist rimonabant also inhibited extinction of conditioned fear (Chhatwal et al., 2009). Interestingly CCK has been shown to increase the excitability of dentate gyrus granule cells (Brooks & Kelly, 1985) and amygdala fast-spiking interneurons (Chung & Moore, 2009).

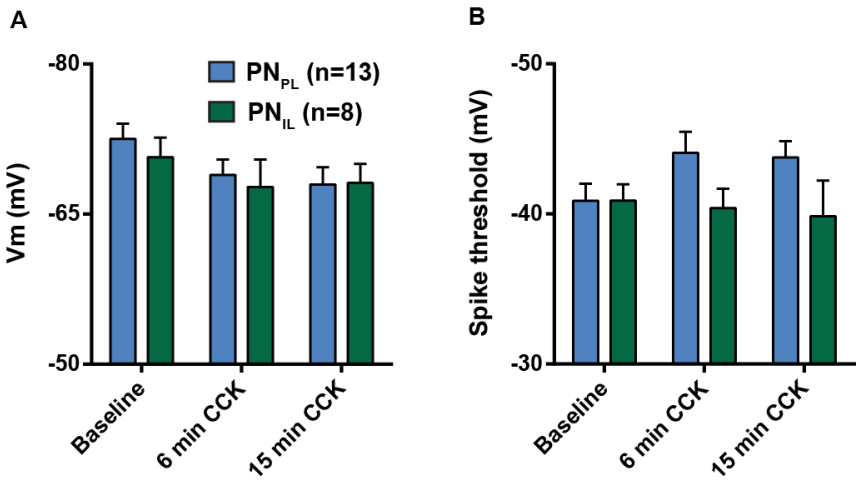

Figure 25. Application of CCK increases AP Threshold in a cell type specific manner. (**A**) CCK (1μM) does not significantly affect pyramidal cell resting membrane potential. (PN_{PL} n = 13; PN_{PL} n = 8; Two-way ANOVA $_{F2,\ 54}$ = 2.20, $p > 0.05$). (**B**) CCK increases spike threshold in PN_{PL}s but not PN_{IL}s PN_{PL} n = 13; PN_{PL} n = 8; Two-way ANOVA $_{F1,\ 51}$ = 4.91, $p < 0.05$).

Given the projection specific endocannabinoid mediated dis-inhibition and regulation of DGLα expression, the question arises whether CCK signaling is also regulated in a cell type specific manner. Therefore CCK (1μM) was applied during recordings of PN_{PL}s and PN_{IL}s. Analysis of spiking pattern revealed no effect of CCK on the resting membrane potential of both cell types (PN_{PL} n = 13; PN_{PL} n = 8; Two-way ANOVA $_{F2,\ 54}$ = 2.20, $p > 0.05$). However, CCK decreased spike threshold in PN_{PL}s but not in PN_{IL}s (PN_{PL} n = 13; PN_{PL} n = 8; Two-way ANOVA $_{F1,\ 51}$ = 4.91, $p < 0.05$). This asymmetric increase in excitability further supports the idea that activity of pyramidal cells is regulated in a cell type specific manner, depending on long-range axonal projection targets.

5. 2. 9. Discussion - additional results

5. 2. 9. 1. CCK_L→CCK_L synapses

Interconnectivity of CCK_Ls is very high with a connection probability of more than 80%. It suggests that a tight network is formed by these interneurons. Interestingly, synapses were not only chemical but also electrical in nature, as precisely time locked simultaneous postsynaptic responses following presynaptic voltage changes were observed. However, due to the experimental design and postsynaptic recordings mostly carried out in voltage clamp mode, a coupling coefficient could not be calculated.

On first sight gap junctions are clashing with GABAergic synaptic transmission. But, as inhibitory transmission had facilitating short-term plasticity dynamics for both tested frequencies, this could lead to a short and precisely timed window during which CCK_Ls are enabled to fire action potentials.

Consistent with findings from CCK_L→$PN_{PL/IL}$ pairs, strongly facilitating CCK_L→CCK_L synapses, compared to depressing dynamics in CCK_L→PN_{IL} and a facilitating-depressing time course in CCK_L→PN_{PL} pairs indicate that short-term plasticity is indeed dependent on the postsynaptic cell type.

Moreover, CCK_L→CCK_L synapses express the weakest form of DSI in all tested groups but synaptic transmission can be completely blocked with application of the CB1 agonist WIN, similarly to what was observed in CCK_L→$PN_{PL/IL}$ pairs. This argues for a generic expression of CB1Rs at CCK_L terminals and further supports the idea that postsynaptic mechanisms regulate the cell type specificity in DSI.

5. 2. 9. 2. Cell-type specific expression of DSI with extracellular stimulation

Results of this separate set of experiments confirm that the expression of DSI is differentially regulated in PN_{IL}s and PN_{PL}s. Tendencies were similar, yet absolute suppression of inhibition was smaller, as extracellular stimulation recruited a variety of local interneurons. These results indicate that even

within a broad spectrum of inhibitory input, activity dependent retrograde suppression of inhibition is significantly different in PN_{IL}s and PN_{PL}s.

5. 2. 9. 3. Effects of CCK on excitability of PN_{PL}s and PN_{IL}s

Given the role of PN_{PL} and PN_{IL} activity in extinction learning, the observed endocannabinoid mediated dis-inhibition in PN_{IL}s opens the obvious question about a mechanism that regulates the activity of PN_{PL}s. Application of the neuropeptide CCK resulted in a decreased spike threshold in PN_{PL}s only, suggesting that CCK might specifically regulate excitability in PN_{PL}s. This is consistent with the literature, reporting that injection of CCK inhibits extinction learning whereas endocannabinoids are required for extinction of conditioned fear (Chhatwal et al., 2009). Strikingly, evidence suggests that the endocannabinoid system is linked to CCK and that the release of endocannabinoids might be triggered by a direct or indirect activation via CCK (Bowers & Ressler 2015). Yet, nothing is known about underlying mechanisms and therefore lot more questions are opened for future directions in this field.

7. DISCUSSION

7. 1. Functional and structural plasticity at GABAergic synapses

By recording mIPSCs in BA principle neurons after behavioral training I found that fear conditioning induced an increase in mIPSC frequency and charge transfer. Interestingly, data from Yu Kasugai and Francesco Ferraguti show that these results correlate with an enlargement of synaptic area and a rearrangement of $GABA_A$ receptor subunit composition. Together this suggests that fear conditioning induced a strengthening of GABAergic synapses.

Enhanced mIPSC frequency might be explained by presynaptic factors such as increases in the number of synapses or vesicles. Moreover, data indicate that postsynaptic alterations could be the reason for elevated levels of charge transfer, which was rather due to slower kinetics than changes in amplitude and remarkably correlated with a rearrangement in receptor subunit composition. Together this is a first indication for a common mechanism underlying functional and structural plasticity.

Both, increases in mIPSC charge transfer as well as synaptic enlargement were detectable immediately after conditioning as well as 24 h later. However, enhanced mIPSC frequency was only observed 24 h post conditioning. Therefore, a frequency change could reflect slower mechanisms of synaptic plasticity or it could be induced by entirely different processes such as learning versus memory consolidation.

Interestingly, extinction training reversed fear conditioning-induced functional and structural plasticity. Previously, it has been shown that extinction is not an erasure of fear memory but an independent learning process (Myers & Davis 2007, Quirk & Mueller 2008, Herry 2010). Therefore, one possible interpretation could be, that findings do not reflect correlates of the actual memory trace but that a fear conditioning induced strengthening of GABAergic synapses may rather be important for the balance of excitation and inhibition.

In contrast to findings in basal amygdala, no overall changes in mIPSCs were detected in LA neurons (structural plasticity was not investigated), which can be explained by two obvious reasons. First, it could be that fear conditioning does not induce GABAergic plasticity in lateral amygdala at all. Second, and more probable, changes in inhibitory transmission could remain undetected in mIPSC recordings and might be differentially organized in basal and lateral amygdala. One possibility could be that plasticity is rather short lasting and occurs simultaneously with the convergence of sensory input during conditioning but does not lead to a remodeling of synapses.

Another factor could be the involvement of different interneuron subtypes. In whole cell configuration synaptic inputs closer to the recording site might dominate the results. Therefore, plasticity of dendritically targeting interneurons could be masked.

Furthermore, changes could be antagonistic and organized in a cell type specific manner. In this scenario a net effect may be close to zero and recordings of unidentified neurons could not reveal distinct changes.

7. 1. 1. Advantages and disadvantages of ex vivo mIPSC recordings

Whole-cell patch clamp mIPSC recordings after behavioral training are a relatively easy method to detect synaptic plasticity in correlation with learning. Changes in mIPSCs frequency can be a first indication that the number of synapses or vesicles increased or decreased. Alterations in amplitude may suggest a strengthening or weakening of synaptic transmission and changes in mIPSC kinetics point to the direction of modifications in receptor subunit composition. However, these read-outs are rather correlative hints and may have other reasons. Furthermore, this method is highly sensitive to minute and partly uncontrollable changes, such as slice quality, preparations of new batches of recording solutions and maybe even seasonal changes for the animal. Therefore it is necessary to always intermingle behavioral groups to avoid drifts being misinterpreted as training effects.

A factor that could add more specificity to this approach would be the identification of recorded cell types. In the basal amygdala fear and extinction neurons have been identified (Herry et al. 2009) which have opposing activity

patterns during high fear and low fear states. Although inhibition is often broad (Liu et al., 2010; Bock et al., 2011; Hofer et al., 2011; Harris & Mrsic-Flogel, 2013) it cannot be excluded that inhibitory input is cell type specific in this case and therefore regulated in opposite directions. Thus, results of this project represent a net effect and have to be interpreted as a population overview on GABAergic transmission following fear conditioning and extinction. This aspect strongly influenced the design of project number two.

7. 2. Cell type specific regulation of GABAergic short-term plasticity

To answer the question whether CCK_Ls provide selective input onto PN_{IL}s and PN_{PL}s that could lead to a switch of activity between these two amygdala output pathways I carried out targeted whole-cell paired recordings. Interestingly, no differences were observed on the level of absolute connectivity but short-term plasticity and in particular endocannabinoid mediated suppression of inhibition suggested a cell type specific regulation of inhibition. $CCK_L \rightarrow PN_{IL}$ synapses exhibited strongest DSI, which is consistent with robust depression upon presynaptic high frequency spike trains. In contrast, lower levels of DSI and facilitating-depressing short-term plasticity dynamics were observed in $CCK_L \rightarrow PN_{PL}$ pairs. The third and distinct type of synapses was examined within networks of CCK_Ls. In line with previous studies, showing that in the amygdala the endocannabinoid synthesis enzyme DGLα is preferentially and in highest levels expressed in pyramidal cells (Yoshida e al., 2011), $CCK_L \rightarrow CCK_L$ synapses displayed the weakest form of DSI and strongly facilitating compound IPSCs in response to presynaptic action potential bursts. Together, these results suggest that inhibition by CCK_Ls is organized in a cell type specific manner, differentiating between distinct types of PNs and also interneuron-interneuron connections.

Strikingly, all three types of synapses were suppressed by bath application of the CB1R agonist WIN with similar strength and time course. This suggests, that cell type specific effects are not due to different levels of presynaptic CB1 receptors. Moreover, immunohistochemical analysis of the presynaptic endocannabinoid degradation enzyme MGL revealed no differences in expression levels at CB1-positive fibres opposing PN_{IL}s or PN_{PL}s. However,

the postsynaptic synthesizing enzyme DGLα was found in higher levels at synaptic contacts onto PN_{IL}s. In conclusion, enzyme levels as well as the effect of WIN bath-application strongly suggest a postsynaptic mechanism underlying the differential expression of DSI.

During extinction learning, in the transition from a high fear to a low fear state, which is correlated with a switch of activity from PN_{PL}s towards PN_{IL}s, cell-type specific endocannabinoid signaling and CCK_Ls may be important for contrast enhancement between these amygdala output pathways. Findings cannot explain the initiation of this switch in activity, as endocannabinoid release is activity dependent. However, this mechanism could tip the balance between activity of PN_{PL}s and PN_{IL}s.

Cell type specific retrograde signaling might be a general mechanism to turn uniform connectivity asymmetric in order to achieve rapid adaptations of network activity. CB1Rs are highly abundant in the CNS and therefore may contribute to learning and memory processes in many brain regions. Together with the presynaptic target selectivity of CCKs that has been described in entorhinal cortex and hippocampus (Varga et al., 2010; Dudok et al., 2015), these interneurons provide a high level of complexity, which may be important for the precise control of PN output.

7. 2. 1. The role of amygdala CCKs within the local GABAergic network

It has been previously suggested that the release of GABA onto BLA PNs is time-, domain-, and sensory-specific (Bienvenu et al., 2012). Furthermore, BLA interneurons are major targets of neuromodulatory systems and tightly control amygdala principal neuron activity (Ehrlich et al., 2009). It suggests a highly complex organization of inhibitory networks, which contributes to the fine-tuning of PN output by redistributing activity amongst cell types and cell compartments in a very specific manner. In line with this idea is the finding of a cell-type specific regulation of DSI. This mechanism may allow for rapid adaptations of pyramidal cell activity and could complement functions of other GABAergic neurons in fear networks. Whereas PV- and SOM-expressing

interneurons have been shown to gate associative learning by disinhibitory mechanisms (Wolff et al., 2014), CCK_Ls might provide the requirements to tip the balance of activity in the network towards PN_{PL}s or PN_{IL}s. However, it remains to be investigated how the switch of activity is initiated as the release of endocannabinoids is activity dependent.

Another factor of complexity is added by data from Chung & Moore (2009), showing that the neuropeptide CCK excites fast-spiking interneurons in BLA. Moreover, CCK-B receptor expression co-localizes with parvalbumin, calbindin and calretinin (Bowers & Ressler, 2015), which is especially interesting as it was also suggested that CCK activates the cannabinoid system via direct or indirect mechanisms. Therefore, CCK interneurons might have a central role in balancing the activity of local amygdala networks.

7. 2. 2. Amygdala CCK_Ls in comparison to CCKs in other brain regions

One major argument for exploring the potential asymmetries in inhibitory input from CCK_Ls onto $PN_{IL/PL}$s was the cell type specific inhibition of projection neurons by CB1R/VGlut3-expressing CCK interneurons in entorhinal cortex (Varga et al., 2010). Yet, in amygdala no differences in absolute connectivity were observed, although it cannot be excluded that CCK_Ls exhibit similar target-selectivity by avoiding PNs projecting to other brain regions than mPFC.

Recently, it has been shown that CCKs selectively target cellular subcompartments in hippocampus. Somatically targeting interneurons expressed higher levels of CB1Rs compared to dendritically targeting CCKs. Consistently, efficacy of endocannabinoid signaling was higher at somatic versus dendritic synapses (Dudok et al., 2015). Therefore, I analyzed IPSC rise time and it's correlation with conductance and DSI to get indications about electrotonic filtering due to a variation in the relative distance of synapses from the recording site. However, rise time did not correlate with conductance or DSI and neither correlated conductance with DSI. These results suggest a homogeneous distribution of synaptic location and that in the recorded population of CCK_Ls DSI levels are not dependent on subtypes of CCK interneurons targeting distinct subcellular domains with different levels

of CB1Rs at presynaptic axon terminals. Together with pharmacological and immunohistochemical data on MGL and DGLα levels, results indicate that the cell-type specific expression of DSI is due to a postsynaptic expression mechanisms. Hence, amygdala CCK_Ls are contrasting other CCK-expressing interneurons with a different level of cell-type specificity.

Furthermore, paired recordings with hippocampal CCKs have shown that IPSCs have a low success rate, long latency and high jitter (Hefft & Jonas, 2005), which does not apply to amygdala CCK_L→PN synapses, where I observed precisely timed IPSCs with short latency and high success rate. Therefore, one possible interpretation could be that amygdala CCK_Ls are designed differentially to meet another set of demands in fear circuits.

7. 2. 3. Strengths and weaknesses of targeted paired-recordings in vitro

The intersectional strategy allowed for the identification of CCK interneurons in slices. However, it has to be considered, that cross breeding three mouse lines resulted in one out of eight animals, that could be used for experiments. Furthermore, via injection of retrograde tracers in a small surgical procedure, specific types of projection neurons could be targeted for recordings. This approach allows drawing conclusions on the dynamic regulation of identified micro-circuits, however, it is missing the behavioral component. We decided not aim for *ex vivo* experiments for two reasons. First, adding a CS only, a fear conditioned and an extinguished group to this project would not be feasible in a reasonable amount of time. Second and more importantly, long-term changes involving CCK interneurons might occur with behavioral training, as recent data indicate (Trouche et al., 2014), however, DSI is a reversible short-term plasticity mechanism, that leads to rapid changes of synaptic input and it is not clear whether learning induces any associated changes that could be detected in a slice. Moreover, the really interesting question would be the relevance of this mechanism *in vivo* and whether or how DSI could lead to an asymmetric dis-inhibition. Here I see the clear advantages and limitations of this *in vitro* method. On one hand the maximum on a behavioral level is reached by recording from cell populations with identified roles in fear learning or maybe experimenting *ex vivo*. On the other hand, paired recordings in slices can answer very distinct questions on a

mechanistic level. For example, asymmetries in DSI could not be detected with single unit recordings. In conclusion, I think that slice recordings are a highly relevant method to study specific questions of circuit mechanisms.

7. 2. 3. Future directions

First of all, can one CCK_L inhibit PN_{IL}s and PN_{PL}s? Triple labeling and triple-recordings of PN_{IL}s, PN_{PL}s and CCK_Ls were performed, however in a reasonable amount of time it was not feasible to titrate the volume of injected beads in order to have no overlap at the injection sites but an acceptable number of labeled neurons in the amygdala that would allow for patch-clamp recordings of neighboring neurons. An alternative strategy could be the anatomical reconstruction of a biocytin filled CCK_Ls, double injection of retrograde tracers and analysis under the confocal microscope.

What is the physiological activity of CCK_Ls? So far, nothing is known about activity of amygdala CCK interneurons *in vivo* and during fear behavior. Answering this question would be important to draw conclusions about the relevance of endocannabinoid-mediated dis-inhibition. As CCK can also be detected in amygdala pyramidal cells, an intersectional approach is required for targeting CCK interneurons specifically. Leak proof Cre-Flp dependent viral vectors, expressing channelrhodopsin or Arch in a cell type specific manner have been developed very recently and could allow for targeted single unit recordings.

An optogenetic approach would also allow for CCK manipulations during behavior. However, basal amygdala CCK interneurons can be divided in at least 2 subclasses, expressing CB1Rs or VIP and/or calretinin and might have diverse functions. Moreover, it is not clear whether endocannabinoid mediated suppression of inhibition is functional when axon terminals are stimulated with channelrhodopsin. Channelrhodopsin is an unselective cation channel and therefore calcium influx might occur despite binding of endocannabinoids. This would need further testing in acute brain slices. Alternatively loss of function experiments by inhibiting the activity of CCK interneurons with Arch could give insight on the functional role of CCK interneurons *in vivo*.

Another burning question would be the identity of presynaptic input onto CCK interneurons. Are CCK interneurons excited by local principal neurons and which brain areas project onto them? Answering this question would shed light on the activity of this GABAergic population and could be achieved by an intersectional rabies strategy, which is not available yet.

Finally, an interesting question that could be answered in a relatively easy experiment, involving retrograde tracing, immunohistochemistry and confocal microscopy, would be whether CCK-B receptors are expressed differentially in PN_{IL}s and PN_{PL}s. However, to understand the possible interactions of CCK and endocannabinoids, a lot more research is necessary on the release of CCK under physiological conditions and associated functional mechanisms.

8. ACKNOWLEDGEMENTS

I would like to cordially thank the following people:

Andreas Lüthi – you were a great and inspiring PhD supervisor and always supporting and motivating me with creative ideas, your passion for science and the right amount of challenges. I'm so grateful for the time in your lab and everything I have learned there!

Josef Bischofberger and **Rainer Friedrich** – a big thank you for supporting me with lots of ideas during thesis committee meetings and taking the time to read and evaluate my thesis!

Francesco Ferraguti and **Yu Kasugai** – thank you so much for this collaboration!

Sabine Krabbe, **Jan Gründemann**, **Jackie Wamsteeker**, **Kristine Bylund** and **Tingjia Lu** – guys, thanks for all your help and support! I couldn't have done it without you! Also, you are a big part of the reason why (even during rough times) every day I was looking forward to going to the lab.

Ingrid Ehrlich – thank you so much for teaching me how to patch and the warm welcome during my first weeks at the FMI!

The Lüthi lab – thanks a lot for making this lab a great working place, being helpful, understanding and supportive! I had an unforgettable time.

The animal, imaging and **histology facility** – an enormous thank you for your help and support!

My closest family - **Mama**, **Daniela**, **Wolfgang** & **Geli** & **Gerhard** & **Wolfi** – I will always be thankful to you for listening and telling me that everything is going to be fine! **Papa** – even though you're not here anymore, I would like to thank you so much for teaching me that it's always worth to follow your passion!

The 2 best BFFs one could ever have, **Silvia** und **Julia** – thanks for always being there for me and cheering me up!

9. REFERENCES

Aggleton, J. P. The Amygdala, a functional analysis. *Oxford University Press* (2000).

Armstrong, C. & Soltesz, I. Basket cell dichotomy in microcircuit function. *J. Physiol*. **590**, 683-694 (2003)

Arruda-Carvalho, M. & Clem, R. L. Pathway-Selective Adjustment of Prefrontal-Amygdala Transmission during Fear Encoding. *Journal of Neuroscience* **34**, 15601–15609 (2014).

Bailey, C. H. & Chen, M. Long-term sensitization in *Aplysia* increases the number of presynaptic contacts onto the identified gill motor neuron L7. *Proc. Natl Acad. Sci. USA* **85**, 9356–9359 (1988).

Bailey, C. H. & Chen, M. Morphological basis of long-term habituation and sensitization in *Aplysia*. *Science* **220**, 91–93 (1983).

Bailey, C. H. & Kandel, E. R. Structural changes accompanying memory formation. *Ann. Rev. Physiol*. **55**, 397–426 (1993).

Bauer, E. P., Schafe, G. E. & LeDoux, J. E. NMDA receptors and L-type voltage-gated calcium channels contribute to long-term potentiation and different components of fear memory formation in the lateral amygdala. *Journal of Neuroscience* **22**, 5239–5249 (2002).

Bienvenu, T. C. M., Busti, D., Magill, P. J., Ferraguti, F. & Capogna, M. Cell-Type-Specific Recruitment of Amygdala Interneurons to Hippocampal Theta Rhythm and Noxious Stimuli In Vivo. *Neuron* **74**, 1059–1074 (2012).

Bissiere, S., Humeau, Y. & LUthi, A. Dopamine gates LTP induction in lateral amygdala by suppressing feedforward inhibition. *Nat. Neurosci.* **6**, 587–592 (2003).

Blitz, D. M., Foster, K. A. & Regehr, W. G. Short-term synaptic plasticity: a comparison of two synapses. *Nat Rev Neurosci* **5**, 630–640 (2004).

Bock, D. D. *et al.* Network anatomy and in vivo physiology of visual cortical neurons. *Nature* **471**, 177–182 (2011).

Bourne, J. N. & Harris, K. M. Coordination of size and number of excitatory and inhibitory synapses results in a balanced structural plasticity along mature hippocampal CA1 dendrites during LTP. *Hippocampus* **21**, 354–373 (2010).

Bowers, M. E. & Ressler, K. J. Interaction between the Cholecystokinin and Endogenous Cannabinoid Systems in Cued Fear Expression and Extinction Retention. *Neuropsychopharmacology* **40**, 688–700 (2015).

Brooks, P. A. & Kelly, J. S. Cholecystokinin as a Potent Excitant of Neurons of the Dentate Gyrus of Rats. *Annals of the New York Academy of Sciences* **448**, 361–374 (1985).

Brown, S. P. & Hestrin, S. Intracortical circuits of pyramidal neurons reflect their long-range axonal targets. *Nature* **457**, 1133–1136 (2009).

Burgos-Robles, A., Vidal-Gonzalez, I. & Quirk, G. J. Sustained conditioned responses in prelimbic prefrontal neurons are correlated with fear expression and extinction failure. *Journal of Neuroscience* **29**, 8474–8482 (2009).

Caroni, P., Donato, F. & Muller, D. Structural plasticity upon learning: regulation and functions. *Nat Rev Neurosci* **13**, 478–490 (2012).

Castillo, P. E., Chiu, C. Q. & Carroll, R. C. Long-term plasticity at inhibitory synapses. *Current Opinion in Neurobiology* **21**, 328–338 (2011).

Chen, J. L. *et al.* Clustered Dynamics of Inhibitory Synapses and Dendritic Spines in the Adult Neocortex. *Neuron* **74**, 361–373 (2012).

Chevaleyre, V., Takahashi, K. A. & Castillo, P. E. Endocannabinoid-mediated synaptic plasticity in the CNS. *Annu. Rev. Neurosci.* **29**, 37–76 (2006).

Chhatwal, J. P. *et al.* Functional Interactions between Endocannabinoid and CCK Neurotransmitter Systems May Be Critical for Extinction Learning. *Neuropsychopharmacology* **34**, 509–521 (2008).

Chhatwal, J. P. Regulation of Gephyrin and GABAA Receptor Binding within the Amygdala after Fear Acquisition and Extinction. *J. Neurosci.* **25**, 502–506 (2005).

Chung, L. & Moore, S. D. Cholecystokinin excites interneurons in rat basolateral amygdala. *Journal of Neurophysiology* **102**, 272–284 (2009).

Collingridge, G. L., Peineau, S., Howland, J. G. & Wang, Y. T. Long-term depression in the CNS. *Nat Rev Neurosci* **11**, 459–473 (2010).

Diana, M. A. & Marty, A. Endocannabinoid-mediated short-term synaptic plasticity: depolarization-induced suppression of inhibition (DSI) and depolarization-induced suppression of excitation (DSE). *Br. J. Pharmacol.* **142**, 9–19 (2004).

Dudok, B. *et al.* Cell-specific STORM super-resolution imaging reveals nanoscale organization of cannabinoid signaling. *Nature Neurosci* **18**, 75–86 (2014).

Ehrlich, I., Humeau, Y., Grenier, F., Ciocchi, S., Herry, C., Lüthi, A. Amygdala Inhibitory Circuits and the Control of Fear Memory. *Neuron* **62**, 757–771 (2009).

Eyre, M. D., Renzi, M., Farrant, M. & Nusser, Z. Setting the time course of inhibitory synaptic currents by mixing multiple GABA(A)R α subunit isoforms. *Journal of Neuroscience* **32**, 5853–5867 (2012).

Fagiolini, M. & Hensch, T. K. Inhibitory threshold for critical-period activation in primary visual cortex. *Nature* **404**, 183–186 (2000).

Fanselow, M. S. & Poulos, A. M. The Neuroscience of Mammalian Associative Learning. *Annu. Rev. Psychol.* **56**, 207–234 (2005).

Freund, T. F. Interneuron Diversity series: Rhythm and mood in perisomatic inhibition. *Trends in Neurosciences* **26**, 489–495 (2003).

Galarreta, M., Iyi, F. E., Szabo, G. B. & Hestrin, A. S. Electrical coupling among irregular-spiking GABAergic interneurons expressing cannabinoid receptors. *Journal of Neuroscience* **24**, 9770–9778 (2004).

Gao, Y. *et al.* Loss of Retrograde Endocannabinoid Signaling and Reduced Adult Neurogenesis in Diacylglycerol Lipase Knock-out Mice. *Journal of Neuroscience* **30**, 2017–2024 (2010).

Geracitano, R., Fischer, D., Kasugai, Y., Ferraguti, F. & Capogna, M. Functional expression of the GABAA receptor α2 and α3 subunits at synapses between intercalated medial paracapsular neurons of mouse amygdala. *Front. Behav. Neurosci.* **6**, (2012).

Graham, B. M. & Milad, M. R. Translational Research in the Neuroscience of Fear Extinction: Implications for Anxiety Disorders. *The American journal of psychiatry* **168**, 1255–1265 (2011).

Granger, A. J. & Nicoll, R. A. Expression mechanisms underlying long-term potentiation: a postsynaptic view, 10 years on. *Philosophical Transactions of the Royal Society of London B: Biological Sciences* **369**, 20130136 (2014).

Grubb, M. S. & Burrone, J. Activity-dependent relocation of the axon initial segment fine-tunes neuronal excitability. *Nature* **465**, 1070–1074 (2010).

Harris, K. D. & Mrsic-Flogel, T. D. Cortical connectivity and sensory coding. *Nature* **503**, 51–58 (2013).

Hashimotodani, Y., Ohno-Shosaku, T., Maejima, T., Fukami, K. & Kano, M. Pharmacological evidence for the involvement of diacylglycerol lipase in depolarization-induced endocanabinoid release. *Neuropharmacology* **54**, 58–67 (2008).

Hefft, S. & Jonas, P. Asynchronous GABA release generates long-lasting inhibition at a hippocampal interneuron–principal neuron synapse. *Nat. Neurosci.* **8**, 1319–1328 (2005).

Heldt, S. A. & Ressler, K. J. Training-induced changes in the expression of GABAA-associated genes in the amygdala after the acquisition and extinction of Pavlovian fear. *Eur J Neurosci* **26**, 3631–3644 (2007).

Hensch, T. K. Critical period plasticity in local cortical circuits. *Nat Rev Neurosci* **6**, 877–888 (2005).

Hensch, T. K. *et al.* Local GABA circuit control of experience-dependent plasticity in developing visual cortex. *Science* **282**, 1504–1508 (1998).

Herry, C. & Johansen, J. P. Encoding of fear learning and memory in distributed neuronal circuits. *Nat. Neurosci.* **17**, 1644–1654 (2014).

Herry, C., Ferraguti, F., Singewald, N., Letzkus, J. J., Ehrlich, I., Lüthi. A. Neuronal circuits of fear extinction. *Eur J Neurosci* **31**, 599–612 (2010).

Herry, C., Ciocchi, S., Senn, V., Demmou, L., Müller, C., Lüthi, A. Switching on and off fear by distinct neuronal circuits. *Nature* **454**, 600–606 (2008).

Hofer, S. B., Ko, H., Pichler, B., Vogelstein, J., Ros, H., Zeng, H., Lein, E., Lesica, N. A., Mrsic-Flogel, T. D. Differential connectivity and response dynamics of excitatory and inhibitory neurons in visual cortex. *Nature Neurosci* **14**, 1045–1052 (2011).

Holtmaat, A. J., Trachtenberg, J. T., Wilbrecht, L., Shepherd, G. M., Zhang, X., Knott, G. W., Svoboda., K. Transient and persistent dendritic spines in the neocortex in vivo. *Neuron* **45**, 279–291 (2005).

Holtmaat, A. & Svoboda, K. Experience-dependent structural synaptic plasticity in the mammalian brain. *Nat Rev Neurosci* **10**, 647–658 (2009).

Hoover, W. & Vertes, R. Anatomical analysis of afferent projections to the medial prefrontal cortex in the rat. *Brain Struct Funct* **212**, 149–179 (2007).

Kandel, E. R., Schwartz, J. H., Jessell, T. M. Principles of neural science, 4/e. *McGraw-Hill* 1227-1279 (2000).

Kasugai, Y., Swinny, J. D., Roberts, D. N., Dalezios, Y., Fukazawa, Y., Sieghart, W., Shigemoto, R., Somogyi, P. Quantitative localisation of synaptic and extrasynaptic GABAA receptor subunits on hippocampal pyramidal cells by freeze-fracture replica immunolabelling. *Eur J Neurosci* **32**, 1868–1888 (2010).

Katona, I., Rancz, E. A., Acsady, L., Ledent, C., Mackie, K., Hajos, N., Freund, T. F. Distribution of CB1 cannabinoid receptors in the amygdala and their role in the control of GABAergic transmission. *J. Neurosci.* **21**, 9506–9518 (2001).

Kaufmann, W., Matsui, K., Jeromin, A., Nerbonne, J. & Ferraguti, F. Kv4.2 potassium channels segregate to extrasynaptic domains and influence intrasynaptic NMDA receptor NR2B subunit expression. *Brain Struct Funct* **218**, 1115–1132 (2013).

Kuba, H., Oichi, Y. & Ohmori, H. Presynaptic activity regulates Na+ channel distribution at the axon initial segment. *Nature* **465**, 1075–1078 (2010).

Lai, C. S. W., Franke, T. F. & Gan, W.-B. Opposite effects of fear conditioning and extinction on dendritic spine remodelling. *Nature* **483**, 87–91 (2012).

Le Be, J. V. & Markram, H. Spontaneous and evoked synaptic rewiring in the neonatal neocortex. *PNAS* **103**, 13214–13219 (2006).

Lamprecht, R. & LeDoux, J. Structural plasticity and memory. *Nat Rev Neurosci* **5**, 45–54 (2004).

Lamsa, K., Heeroma, J. H. & Kullmann, D. M. Hebbian LTP in feed-forward inhibitory interneurons and the temporal fidelity of input discrimination. *Nat. Neurosci.* **8**, 916–924 (2005).

LeDoux, J. E. Emotion circuits in the brain. *Annu. Rev. Neurosci.* **23**, 155–184 (2000).

LeDoux, J. E., Cicchetti, P., Xagoraris, A. & Romanski, L. M. The lateral amygdaloid nucleus: sensory interface of the amygdala in fear conditioning. *J. Neurosci.* **10**, 1062–1069 (1990).

Liu, B.-H., Li, P., Sun, Y. J., Li, Y.-T., Zhang, L. I., Tao, H. W. Intervening inhibition underlies simple-cell receptive field structure in visual cortex. *Nature Neurosci* **13**, 89–96 (2009).

Luchicchi, A. & Pistis, M. Anandamide and 2-arachidonoylglycerol: Pharmacological Properties, Functional Features, and Emerging Specificities of the Two Major Endocannabinoids. *Mol Neurobiol* **46**, 374–392 (2012).

Maffei, A. The Many Forms and Functions of Long Term Plasticity at GABAergic Synapses. *Neural Plasticity* **2011**, 1–9 (2011).

Makkar, S. R., Zhang, S. Q. & Cranney, J. Behavioral and Neural Analysis of GABA in the Acquisition, Consolidation, Reconsolidation, and Extinction of Fear Memory. *Neuropsychopharmacology* **35**, 1625–1652 (2010).

Malenka, R. C. & Bear, M. F. LTP and LTD: an embarrassment of riches. *Neuron* **44**, 5–21 (2004).

Maren, S. & Quirk, G. J. Neuronal signalling of fear memory. *Nat Rev Neurosci* **5**, 844–852 (2004).

Marsicano, G. *et al.* The endogenous cannabinoid system controls extinction of aversive memories. *Nature* **418**, 530–534 (2002).

Mascagni, F. & McDonald, A. J. Immunohistochemical characterization of cholecystokinin containing neurons in the rat basolateral amygdala. *Brain Research* **976**, 171–184 (2003).

Matsuzaki, M., Honkura, N., Ellis-Davies, G. C. R. & Kasai, H. Structural basis of long-term potentiation in single dendritic spines. *Nature* **429**, 761–766 (2004).

McDonald, A. J. & Mascagni, F. Immunohistochemical characterization of somatostatin containing interneurons in the rat basolateral amygdala. *Brain Research* **943**, 237–244 (2002).

McDonald, A. J. & Mascagni, F. Localization of the CB1 type cannabinoid receptor in the rat basolateral amygdala: high concentrations in a subpopulation of cholecystokinin-containing interneurons. *Neuroscience* **107**, 641–652 (2001).

McKernan, M. G. & Shinnick-Gallagher, P. Fear conditioning induces a lasting potentiation of synaptic currents in vitro. *Nature* **390**, 607–611 (1997).

Miyoshi, G. *et al.* Genetic fate mapping reveals that the caudal ganglionic eminence produces a large and diverse population of superficial cortical interneurons. *Journal of Neuroscience* **30**, 1582–1594 (2010).

Möhler, H. Molecular regulation of cognitive functions and developmental plasticity: impact of $GABA_A$ receptors. *J Neurochem* **102**, 1–12 (2007).

Muller, J. F., Mascagni, F. & McDonald, A. J. Postsynaptic targets of somatostatin-containing interneurons in the rat basolateral amygdala. *J. Comp. Neurol.* **500**, 513–529 (2007).

Muller, J. F., Mascagni, F. & McDonald, A. J. Pyramidal cells of the rat basolateral amygdala: Synaptology and innervation by parvalbumin-immunoreactive interneurons. *J. Comp. Neurol.* **494**, 635–650 (2005).

Myers, K. M. & Davis, M. Mechanisms of fear extinction. *Mol Psychiatry* **12**, 120–150 (2007).

Nabavi, S., Fox, R., Proulx, C. D., Lin, J. Y., Trien, R. Y., Malinow, R. Engineering a memory with LTD and LTP. *Nature* **511**, 348–352 (2014).

Nadel, L. & Land, C. Memory traces revisited. *Nat Rev Neurosci* **1**, 209–212 (2000).

Nicoll, R. A. & Malenka, R. C. Contrasting properties of two forms of long-term potentiation in the hippocampus. *Nature* **377**, 115–118 (1995).

Ohno-Shosaku, T., Maejima, T. & Kano, M. Endogenous Cannabinoids Mediate Retrograde Signals from Depolarized Postsynaptic Neurons to Presynaptic Terminals. *Neuron* **29**, 729–738 (2001).

Ostroff, L. E., Cain, C. K., Jindal, N., Dar, N. & LeDoux, J. E. Stability of presynaptic vesicle pools and changes in synapse morphology in the amygdala following fear learning in adult rats. *J. Comp. Neurol.* **520**, 295–314 (2012).

Pape, H. C. & Pare, D. Plastic Synaptic Networks of the Amygdala for the Acquisition, Expression, and Extinction of Conditioned Fear. *Physiological Reviews* **90**, 419–463 (2010).

Quirk, G. J. & Mueller, D. Neural Mechanisms of Extinction Learning and Retrieval. *Neuropsychopharmacology* **33**, 56–72 (2008).

Rainnie, D. G., Mania, I., Mascagni, F. & McDonald, A. J. Physiological and morphological characterization of parvalbumin-containing interneurons of the rat basolateral amygdala. *J. Comp. Neurol.* **498**, 142–161 (2006).

Regehr, W. G., Carey, M. R. & Best, A. R. Activity-Dependent Regulation of Synapses by Retrograde Messengers. *Neuron* **63**, 154–170 (2009).

Rudolph, U. & Möhler, H. Analysis of $GABA_A$ receptor function and dissection of the pharmacology of benzodiazepines and general anaesthetics through mouse genetics. *Annu. Rev. Pharmacol. Toxicol.* **44**, 475–498 (2015).

Rumpel, S., LeDoux, J., Zador, A., Malinow, R. Postsynaptic Receptor Trafficking Underlying a Form of Associative Learning. *Science* **308**, 83–88 (2005).

Sah, P., Westbrook, R. F. & Lüthi, A. Fear conditioning and long-term potentiation in the amygdala: what really is the connection? *Annals of the New York Academy of Sciences* **1129**, 88–95 (2008).

Senn, V., Wolff, S. B. E. Herry, C., Grenier, F., Ehrlich, I., Gründemann, J., Fadok, J. P., Müller, C., Letzkus, J. J., Lüthi, A. Long-Range Connectivity Defines Behavioral Specificity of Amygdala Neurons. *Neuron* **81**, 428–437 (2014).

Sieghart, W. & Sperk, G. Subunit Composition, Distribution and Function of GABA-A Receptor Subtypes. *CTMC* **2**, 795–816 (2002).

Sierra-Mercado, D., Padilla-Coreano, N. & Quirk, G. J. Dissociable roles of prelimbic and infralimbic cortices, ventral hippocampus, and basolateral amygdala in the expression and extinction of conditioned fear. *Neuropsychopharmacology* **36**, 529–538 (2011).

Spampanato, J., Polepalli, J. & Sah, P. Interneurons in the basolateral amygdala. *Neuropharmacology* **60**, 765–773 (2011).

Spejo, A. B. & Oliveira, A. L. R. Synaptic rearrangement following axonal injury: Old and new players. *Neuropharmacology* 1–11 (2014).

Taniguchi, H. *et al.* A Resource of Cre Driver Lines for Genetic Targeting of GABAergic Neurons in Cerebral Cortex. *Neuron* **71**, 995–1013 (2011).

Tanimura, A. *et al.* The Endocannabinoid 2-Arachidonoylglycerol Produced by Diacylglycerol Lipase α Mediates Retrograde Suppression of Synaptic Transmission. *Neuron* **65**, 320–327 (2015).

Trouche, S., Sasaki, J. M., Tu, T. & Reijmers, L. G. Fear extinction causes target-specific remodeling of perisomatic inhibitory synapses. *Neuron* **80**, 1054-65 (2013).

Varga, C., Lee, S. Y. & Soltesz, I. Target-selective GABAergic control of entorhinal cortex output. *Nat. Neurosci.* **13**, 822–824 (2010).

Vyas, A., Mitra, R., Shankaranarayana Rao, B. S. & Chattarji, S. Chronic stress induces contrasting patterns of dendritic remodeling in hippocampal and amygdaloid neurons. *J. Neurosci.* **22,** 6810–6818 (2002).

Wehr, M. & Zador, A. M. Balanced inhibition underlies tuning and sharpens spike timing in auditory cortex. *Nature* **426**, 442–446 (2003).

Wilson, R. I. & Nicoll, R. A. Endogenous cannabinoids mediate retrograde signalling at hippocampal synapses. *Nature* **410**, 588–592 (2001).

Wilson, R. I. & Nicoll, R. A. Endocannabinoid signaling in the brain. *Science* **296**, 678–682 (2002).

Wilson, R. I., Kunos, G. & Nicoll, R. A. Presynaptic Specificity of Endocannabinoid Signaling in the Hippocampus. *Neuron* **31**, 453–462 (2001).

Wolff, S. B. E. *et al.* Amygdala interneuron subtypes control fear learning through disinhibition. *Nature* **509**, 453–458 (2014).

Xu, T. et al. Rapid formation and selective stabilization of synapses for enduring motor memories. *Nature* **462**, 915–919 (2009).

Yang, G., Pan, F. & Gan, W. B. Stably maintained dendritic spines are associated with lifelong memories. *Nature* **462**, 920–924 (2009).

Yoshida, T. *et al.* Unique inhibitory synapse with particularly rich endocannabinoid signaling machinery on pyramidal neurons in basal amygdaloid nucleus. *Proc. Natl. Acad. Sci. U.S.A.* **108**, 3059–3064 (2011).

Yuste, R. & Bonhoeffer, T. Morphological hanges in dendritic spines associated with long-term synaptic plasticity. *Annu. Rev. Neurosci.* **24**, 1071–1089 (2015).